Postprint of: Kupfer S., Zedler L., Guthmuller J., Bode S., Hager M., Schubert U., Popp J., Gräfe S., Dietzek B., Self-healing mechanism of metallopolymers investigated by QM/MM simulations and Raman spectroscopy, PHYSICAL CHEMISTRY CHEMICAL PHYSICS, Vol. 16, iss. 24 (2014), pp. 12422-12432, DOI: 10.1039/C4CP00562G

Self-healing Mechanism of Metallopolymers Investigated by QM/MM Simulations and Raman Spectroscopy

Stephan Kupfer[1,2,§,*], Linda Zedler[1,2,§], Julien Guthmuller[3], Stefan Bode[4,5], Martin D. Hager[4,5], Ulrich S. Schubert[4,5], Jürgen Popp[1,2,6], Stefanie Gräfe[1,2], Benjamin Dietzek[1,2,6*]

[1]*Institute for Physical Chemistry, Friedrich Schiller University Jena, Helmholtzweg 4, 07743, Jena, Germany*

[2]*Abbe Center of Photonics, Friedrich Schiller University Jena*

[3]*Faculty of Applied Physics and Mathematics, Gdansk University of Technology, Narutowicza 11/12, 80233 Gdansk, Poland*

[4]*Laboratory for Organic and Macromolecular Chemistry, Friedrich Schiller University Jena, Humboldtstr. 10, 07743, Jena, Germany*

[5]*Jena Center of Soft Matter, Friedrich Schiller University Jena, Philosophenweg 7, 07743, Jena, Germany*

[6]*Institute for Photonic Technology (IPHT) Jena, Albert-Einstein-Str. 9, 07745, Jena, Germany*

* stephan.kupfer@uni-jena.de

* benjamin.dietzek@ipht-jena.de

§ Both authors contributed equally to this article.

Abstract

The thermally induced self-healing mechanisms in metallopolymers based on *bis*terpyridine complexes of iron(II) sulfate and cadmium(II) bromide, respectively, were studied by means of combined quantum mechanical / molecular mechanical (QM/MM) simulations and Raman spectroscopy. Two possible healing schemes, one based on a decomplexation of the cross-linking complexes and a second one relying on the dissociation of ionic clusters, have been addressed. Temperature-dependent Raman spectroscopy displayed bathochromic shifts of the Raman intensity pattern upon heating. QM/MM simulations on the polymer models assign these alterations to a partial decomplexation of the metal terpyridine complexes, i.e. signals originating from free terpyridine ligands increase upon heating. Thus, a healing mechanisms based on partial decomplexation of the cross-linking complexes is suggested. The possibility that the dissociation of ionic clusters, which are assumed to be present in this class of self-healing polymers, is also responsible for the self-healing process was investigated as well. However, such calculations on model clusters revealed relatively strong binding of the clusters, which renders reversible cluster breaking and reformation upon temperature cycling in the range up to 100 °C unlikely.

1. Introduction

Self-healing materials feature the ability to heal mechanical damage suffered by chemical or physical stress and to (partially) recover their mechanical properties autonomously or upon application of an external stimulus.[1–8] Manifold applications for self-healing materials are conceivable ranging from coatings[9,10], over asphalts[11,12] and to steel alloys[13]. The basic concept behind such functional materials is the generation of a mobile phase, which can subsequently close the crack/scratch.[4] One possibility to obtain self-healing is the utilization of (weak) reversible interactions between specific molecular structures embedded, e.g., in a polymer. In order to provide an ideally unlimited number of healing cycles, such interactions need to be highly reversible. A wide range of chemical and physical interactions fulfil these preliminary conditions, e.g., based on Diels-Alder reactions[1,14,15], on disulfide bonds[16,17], or by means of supramolecular interactions like hydrogen bonds[18–21], ionic interactions[22,23], π–π-interactions[24,25], guest-host interactions[26,27] as well as metal-ligand interactions.[28–30] Depending on the nature of the underlying healing mechanism the recovery of the initial (mechanical) properties can be achieved autonomously or by means of external stimuli, e.g., by irradiation or thermal activation.

A promising approach is to utilize metal-ligand interactions; this principle is also known in nature, e.g., in mussel byssus anchoring the mussel on a substrate, where self-healing based on reversible iron(III) dihydroxy-phenylalanine interactions is observed upon mechanical stress.[31–33] Recently, a variety of self-healing terpyridine metallopolymers cross-linked by different metal salts such as iron(II) sulfate and cadmium(II) chloride, bromide, iodine and acetate have been synthesised, which can be schematically depicted as shown in Figure 1a).[29,30] These polymers are based on a lauryl methacrylat polymer backbone and exhibit pronounced healing properties upon thermal activation at moderate temperatures of approximately 100 °C.

In order to improve on the self-healing properties of such materials it is of uttermost importance to unravel the underlying healing mechanism at a molecular scale. One suited tool to investigate structural alterations during the thermally induced healing process is temperature dependent Raman

spectroscopy.[29,34,35] Furthermore, small angle x-ray scattering (SAXS) measurements provide an interesting opportunity to resolve nano scale structures in polymers.[36,29,30] For example Varley and van der Zwaag proved that nano structures based on ionic clusters contribute to the healing mechanism in ionomers.[37–40] A promising approach to investigate self-healing on a molecular level is provided by theoretical simulations aiming to describe the interactions responsible for the healing process in metallopolymers. However, the enormous size of such macromolecular systems requires the use of mixed quantum mechanical / molecular mechanical (QM/MM) simulations,[41,42] which combine a QM description of the ligands cross-linked by metal salts and a MM description of the polymer backbone.

This work presents a joint theoretical-spectroscopic[43,44,34] guided investigation to study the healing process of selected representative metallopolymers synthesised in the group of U. S. Schubert. Two forms of metallopolymers involving a lauryl methacrylate polymer backbone functionalized by terpyridine ligands and cross-linked by metal salts, namely iron(II) sulfate and cadmium(II) bromide, have been considered. First investigations on these metallopolymers based on SAXS measurements point to the presence of ionic clusters.[29,30] In addition, structural changes during the healing process were monitored by temperature-dependent Raman spectroscopy for the iron(II) sulfate polymer.[29] Herein, the study is extended to the thermally induced self-healing in the cadmium(II) bromide analogue. Moreover, to obtain detailed insight into structural properties and to further unravel the self-healing mechanism with respect to the two concepts based on either metal-ligand interactions (see Figure 1b)) or ionic clusters (see Figure 1c)), QM/MM simulations have been performed. On the one hand, these QM/MM simulations aim at investigating the metal-ligand interactions with respect to the iron(II) sulfate and cadmium(II) bromide cross-linking. Hence, two polymer models, depicted in Figure 1d), comprising more than 630 atoms have been constructed to mimic the metallopolymers. On the other hand, the formation of ionic clusters and a possible contribution to the self-healing mechanism is analysed by means of QM/MM simulations on a polymer models containing nearly 1300 atoms, see Figure 1e).

The theoretical simulations provide the basis to address the origin of the alterations in the experimental Raman intensity pattern during the thermally induced healing process and, hence, to unravel the nature of the underlying self-healing mechanism.

2. Theory and Computational Details

Quantum chemical simulations have been performed for several metallopolymer model systems mimicking lauryl methacrylate polymers containing terpyridine ligands. The polymer models were investigated in a non-cross-linked form, i.e. free terpyridine ligands present, and cross-linked by iron(II) sulfate or cadmium(II) bromide. For each metallopolymer one polymer model featuring a central *bis*terpyridine cross-linking complex (bearing the respective counter ions), two attached methacrylate polymers and two terminal free terpyridine moieties have been created, see Figures 2b) and 3b). These polymer models have been treated using QM/MM[41,42] as implemented in the Gaussian 09[45] program, where the central complex, the counter ions as well as the terminal terpyridine ligands have been described using density functional theory and the lauryl methacrylate at MM level of theory. The geometry, vibrational frequencies, normal coordinates and Raman intensities of the ground state were calculated with the functional B3LYP(15)[46,47] for the QM layer and with the universal force field (UFF) for the MM layer. The B3LYP(15) functional is based on the B3LYP[48,49] functional and combines 15% of exact exchange, 58.5% of non-local B88 exchange and the LYP correlation. The 10-electron non-relativistic effective core potential MDF-10[50] was used with its basis set for the iron atom, that is, 3s, 3p, 3d and 4s electrons are treated explicitly, whereas the two first inner shells are described by the core pseudopotential. For the cadmium atom the non-relativistic MWB-28 core potential was applied (treating the 4s, 4p, 4d and 5s electrons explicitly). The 6-31G(d) double-ζ basis set[51] was employed for the ligands, which was shown to be adequate for the calculation of Raman spectra.[52] To correct for the lack of anharmonicity and the approximate treatment of electron correlation, the harmonic frequencies were scaled by the factor 0.97.[53] To gain insight into the absorption properties, the 150 lowest singlet excited states have been calculated for both polymer models in gas phase as well as in acetonitrile using the polarizable continuum model.[54] Furthermore, resonance Raman spectrum of the iron(II) sulfate metallopolymer was calculated using an excitation wavelength of 647 nm, detailed information concerning the applied theory for calculating RR intensities is provided in Ref. [55–57] and therein.

The model systems we used for calculating the Raman spectra of the metallopolymers are constructed based on the desired repeating unit of the experimental target structure and represent thus the smallest possible unit of the polymer, containing the necessary ingredients for a mechanistic investigation of self-healing: (i) the polymer backbone, assumed to be of minor importance for the self-healing, thus described with lower level in theory; (ii) the complexated metal, being of vital importance for the mechanism and thus described with DFT level of theory; (iii) free ligand attached to the polymer backbone, for reasonable comparison with the complexated metal described on the same level of theory. While this model does certainly not provide the full and most accurate description of the actual experimental polymer, we believe that it mimics the complex system reasonably well.

In order to study interactions within ionic clusters, composed by the positively charged cross-linking complexes and the negatively charged counter ions, two extended polymer models have been created. These models comprise approximately 1300 atoms, in which two of the previously described models have been cross-linked by means of the respective counter ions. To get insight into the thermodynamics of such clusters, relaxed potential energy surfaces (PESs) have been calculated with respect to the distance between one complex and the bridging counter ion of the other complex (*R*, see Figure S1 of the supplementary information). In order to reduce the computational demand of these calculations, the MM layer was extended and contains in addition to the methacrylate polymer also the four terminal terpyridine ligands. The partial geometry optimizations along the coordinate *R* have been carried out using the same functional, basis set, force field, and core potential as stated above.

3. Experimental Methods

Temperature-dependent Raman spectra were recorded using various experimental setups, either a LabRAM HR800 Raman spectrometer (Horiba-Jobin Yvon) or a confocal Raman microscope (model CRM 2000, WITec), both working in backscattering geometry. The LabRAM spectrometer was equipped with a confocal aperture and an upright microscope (Olympus BX40). The Raman excitation laser at 647 nm was provided by a krypton ion laser (Innova 302C, Coherent). Laser power at the sample was < 2 mW. The slit width was set to 100 μm, the pinhole either to 500 μm or to 1000 μm and the scattered light was detected by a liquid-nitrogen-cooled charge coupled device (CCD). The spectral resolution was 2 cm^{-1} for the grating 1800/mm^{-1}. Excitation at 785 nm for the WITec Raman microscope was provided by a single mode diode laser (< 10 mW laser power at the sample). The laser radiation was coupled into a Zeiss microscope and focused onto the sample through a microscope objective (Zeiss EC Epiplan Apochromat 50x/0.95 NA). The spectral resolution was 6 cm^{-1} for the grating 600/mm^{-1}. The sample temperature was adjusted using a Linkam stage (model LTS 350), which was fixed under the microscope objective.

4. Results

The temperature-dependent Raman spectra of the polymer cross-linked by iron(II) sulfate and cadmium(II) bromide are depicted in Figure 2a) and Figure 3a), respectively. Both polymers feature characteristic shifts of the Raman bands in the region between 1450 and 1650 cm^{-1} towards lower wavenumbers upon heating. However, in case of the iron(II) sulfate metallopolymer the shifts are more pronounced (approximately 3 and 4 cm^{-1}) than for the cadmium(II) bromide analogue, where a band shift of 1.4 cm^{-1} is observed. The band shifts are verified by repeatedly measuring the band position at low and high temperature and detecting the maximum of the bands. In comparison to other vibrational resonances which are not affected by heating, the shift was reproducible, always towards lower frequencies and is therefore not due to the limited accuracy of the measurements. To address the origin of the observed spectral shifts with respect to the self-healing properties of the materials, we will discuss in the following two healing mechanisms: The first one is based on a thermal decomplexation of the cross-linking terpyridine complexes, while the second one involves the cleavage of ionic clusters formed by means of the *bis*terpyridine-iron(II) and *bis*terpyridine-cadmium(II) complexes and their anionic counter ions, namely sulfate and bromide.

4.1 Decomplexation

4.1.1 Iron(II) cross-linked polymer

The ground state equilibrium geometry of the iron(II)-cross-linked polymer depicted in Figure 2b), optimized at the QM/MM level of theory, features a linear structure, where the iron-terpyridine complex is located at the center, and the free terpyridine ligands are oriented outwards. A subsequent vibrational analysis proved that the optimized equilibrium geometry is a minimum of the electronic ground state potential energy surface. In contrast to the terpyridine ligands of the iron(II) complex, the uncoordinated ligands feature a trans-configuration of the pyridyl moieties due to electrostatic repulsion of the nitrogen atoms. The structure of the central *bis*terpyridine-iron(II) fragment is slightly distorted by virtue of the sulfate counter-ion binding to the central pyridyl ring

of one terpyridine ligand. This induces a pronounced sp^3-character of the carbon atom connecting the sulfate and in consequence a loss of planarity is observed for this terpyridine ligand. For the carbon-oxygen(sulfate)-bond a length of 1.450 Å was obtained. In case of the nitrogen-iron bonds values of 1.880 (central pyridyl-moiety), 1.988 and 2.001 Å (terminal pyridyl-moieties) were calculated for the planar terpyridine ligand. Due to the electronic and structural alterations induced by the sulfate ion, the corresponding nitrogen-iron bond lengths of the other terpyridine ligand are slightly stretched by approximately 0.025 Å.

The vibrational analysis of the iron(II) metallopolymer allowed to rationalise the temperature-dependent Raman spectra, which reflect structural changes upon heating and, hence, during the self-healing process. In Figure 2a) the Raman scattering intensity pattern is depicted exemplarily for the minimum and the maximum temperatures of 23 and 100 °C. An overall intensity increase upon heating is accompanied by a bathochromic shift of two prominent Raman features, i.e., at 1547 cm^{-1} by 3 cm^{-1} and at 1607 cm^{-1} by 4 cm^{-1} towards lower frequency. The detected shift is reproducible and clearly resolvable within the accuracy of the measurement (see Figure S2a of the supplementary information). The Raman spectrum calculated by means of QM/MM (B3LYP(15)/UFF) illustrated in Figure 2b) is composed of modes of the free terpyridine ligands as well as of the iron(II)-terpyridyl complex, while the lauryl methacrylate polymer does not contribute to the spectrum as the MM region is not assigned any polarizability.

As can be seen from Figure 2a) and b), the dominant experimentally observed Raman bands in the 1450-1700 cm^{-1} region can be assigned to modes of the free ligand and the iron(II)-terpyridyl complex. This band assignment is also in agreement with the measured spectra (Figure S5).[52] The calculated spectrum, Figure 2a) and b), show more pronounced deviations in the 900-1450 region from the experiment. This can be ascribed to the neglect of Raman bands originating from the polymer backbone.

Of particular interest for the investigation of the self-healing mechanisms are the vibrational modes contributing to the Raman spectrum in the range of 1450 and 1620 cm^{-1}, where the bathochromic

shifts have been observed experimentally. On the basis of the frequencies and relative intensities the experimental Raman bands localized at 1468, 1490, 1546, 1558 and 1606 cm^{-1} can be assigned to the calculated Raman bands centered at 1453, 1467, 1584, 1601 and 1669 cm^{-1} (see Figure2a) and b)). This corresponds to a mean absolute deviation (MAD) of 21 cm^{-1}, which is typical at this level of theory.[53] An analysis of the vibrational modes showed that modes localized at the free ligands are lower in energy than the corresponding modes of the complexated terpyridine ligand. This can be seen exemplarily by means of the calculated band structure centered around 1669 cm^{-1}, where the intensity pattern is mainly governed by five modes 1450, 1452, 1461, 1462, and 1463. The mode 1450 at 1658.7 cm^{-1} centered at a free terpyridine ligand corresponds to the complexated terpyridine mode 1452 at 1661.7 cm^{-1}. The mode at 1668.7 cm^{-1} is located at the free terpyridine ligand (mode 1461), the corresponding modes of the complexated ligand are found at 1669.8 and 1670.5 cm^{-1} (mode 1462 and 1463), respectively. The slight bathochromic shift is caused by the distortion of the equilibrium geometry of one complexated terpyridine ligand by virtue of the sulfate counter ion. Hence, the mode of the free ligand is bathochromically shifted by about 0.7 to 3 cm^{-1} with respect to the *bis*terpyridine-iron(II) complex. For other bands, e.g., correlated to the experimental Raman bands at 1546 and 1558 cm^{-1}, even more pronounced shifts of approximately 12.5 cm^{-1} (with respect to the free terpyridine modes 1415 and 1416 and the similar modes in the complex 1422 and 1424) and 13.9 cm-1 (for the free terpyridine modes 1417 and 1418 and the complexated terpyridine modes 1425 and 1428) have been calculated. More detailed information concerning the vibrational modes is given in Table 1 and Figure S3.

The consistent bathochromic shift of the vibrational frequencies of the free terpyridine with respect to the *bis*terpyridine-iron(II) complex indicates to thermal decomplexation. In this case the cross-linking of the metallopolymer is (partially) suspended upon heating and the Raman spectrum is dominated by vibrational modes of the free terpyridine ligands. In order to study the ligand exchange mechanisms further, QM/MM simulations have been performed for a partially dissociated complex, where one terpyridine ligand is removed and the iron(II) is bound to one terpyridine and

the sulfate ion; the structure as well as the simulated Raman spectrum is illustrated in Figure 2c).

Comparing the frequencies of the respective modes localized at the free terpyridine (716, 717, and 733) as well as on the complexated ligand (720, 721, and 739) yields only minor variation with respect to their analogues of the afore described polymer model (vibrational modes are visualized in Figure S4). However, the Raman activity of the complexated modes decreases from the *bis*terpyridine complex (modes 1422, 1424, 1425, 1428, 1452, 1462, and 1463) upon partial decomplexation (modes 720, 721, and 739), see Table 1, while the Raman activities of the free terpyridine ligands are almost unaffected. Hence, the enveloping Raman bands between 1450 and 1620 cm^{-1} are shifted to slightly lower frequencies compared to the bisterpyridine-iron(II) metallopolymer model (Figure 2b)).

In order to evaluate the robustness of the applied computational approach, effects of the XC functional and the basis set on the vibrational frequencies and Raman intensities have been investigated by means of the standard B3LYP functional as well as the 6-311(d) triple-ζ basis set. These simulated Raman spectra show only minor deviations from the spectra obtained by B3LYP(15) and the 6-31G(d) double-ζ basis set, while the qualitatively picture including the red-shift of the free ligand centered modes with respect to the analogous modes of the complex is preserving (see Table S4, Figure S5, and Figure S6 of the supporting information).

Undoubtedly, the calculated vibrational spectra differ on an absolute scale from the experimentally obtained ones. However, *relative shifts* in the calculated spectrum can be very well analyzed. Within the same method and the same basis set, changes in the spectrum induced by modest, stepwise deformation of the geometry – and here in particular the relative coordinate representing the distance between the metal center and the ligand sphere – can be extracted. With our mechanistic model systems, we can contrast the relative shifts in the spectrum for the two mechanisms of interest and compare them to the experimentally observed relative shifts. This allows us to provide a plausible explanation of the experimentally shifts with respect to a thermal decomplexation by comparing the vibrational frequencies and intensities of the complexated terpyridine ligand with the

analogous vibrational modes of the free ligand (formed upon heating).

The absolute frequency of vibrational modes is dependent on the applied computational method (XC functional and basis set).These effects were largely studied in the literature and were shown to be quite systematic.[53,60] Therefore, the frequency shifts can be obtained with higher accuracy than the absolute frequencies. However, the relative shifts might depend on the theoretical method as well. In order to address this issue, we have performed a large number of additional calculations, varying both, the basis set and the functional used in the DFT. We calculated the Raman spectra of all three model systems (iron(II) sulfate metallopolymer, iron(II) sulfate semi-decomplexed metallopolymer, and cadmium(II) bromide metallopolymer) in order to address effects of the basis set as well as of the functional. It was found for all intense modes in the frequency region between 900 and 1800 cm^{-1} of the three model systems that the increase from double to triple-ζ basis set (6-311G(d)) leads to a bathochromic shift of the vibrational frequencies of approximately 10 cm^{-1}, while an increase of the exact exchange in the XC functional from 15 (B3LYP(15)) to 20% (standard B3LYP) leads to a hypochromic shift of approximately 10 cm^{-1}.

The shifts of the modes centered at the complex and the free ligand are preserved, while the frequency of the free ligand modes are found red-shifted to the respective modes loacalized on the complexated ligand, independent of the method or the basis set.

The theoretical investigation of the iron(II) metallopolymer indicates a self-healing mechanism based on a (partial) decomplexation of the cross-linking complexes. This is further supported by Raman spectroscopy on the terpyridine and *bis*terpyridine-iron(II) monomers (see Figure S8 of the supporting information), where a bathochromic shift of 6 cm^{-1} was observed for the Raman features of the terpyridine monomer (1602 cm^{-1}) with respect to the complex (1608 cm^{-1}).

In order to investigate possible resonance enhancement in the Raman spectra, absorption and resonance Raman (RR) spectra were calculated for iron(II) sulfate metallopolymer by means of QM/MM simulations. In the simulation of the absorption spectrum, solely excitations of the free ligands and the complex have been taken into account by means of TDDFT. The calculated

absorption spectrum is in good agreement with the experimental spectrum (in acetonitrile), see Figure 4a). The experimental absorption band centered at 555 nm was found to stem from an intra-ligand excitation (S_4) of the iron(II)-terpyridyl-complex. The excitation energy of the S_4 state is slightly underestimated by 0.05 eV with respect to the experimental absorption maximum. For the measurement of the Raman spectra an excitation wavelength of 647 nm was used, hence, a resonance enhancement due to an excited state is unlikely. Since the Raman signals are measured in solid-state, which consists of a less polar environment, the absorption was further simulated without applying the effects of solvation, see Figure 4b). Consequently, the bright intra-ligand state located at the *bis*terpyridine-iron(II) complex is lowered from 2.18 (S_4, Figure 4a) to 2.12 eV (S_{10}, Figure 4b). These results indicate that effects due to resonance enhancement are of minor importance.

In order to fully exclude a resonance enhancement at the excitation wavelength of 647 nm, the resonance Raman (RR)[55] spectrum using the excited state gradients of the S_{10} (bright $\pi\pi^*$ state at 555 nm) have been calculated using the QM/MM model system with the *bis*terpyridine-iron(II) complex in the center and two free terminal terpyridine ligands. The simulated RR intensity pattern of Figure 2d) shows, as expected from the $\pi\pi^*$ nature of the S_{10} state, exclusively intense modes localized at the bisterpyridine-iron(II) complex. The poor agreement between the calculated RR intensities and the experimental Raman spectra of Figure 2a) and d) indicates a non-resonant scattering process at 647 nm.

4.1.2 Cadmium(II) cross-linked polymer

Analogous to the metallopolymer cross-linked by iron(II) sulfate, a QM/MM model system was constructed, consisting of a DFT layer comprising the central *bis*terpyridine-cadmium(II) complex, the two bromide counter-ions attached to each of the complexated ligands, and the terminal free terpyridine ligands and a MM layer describing the lauryl methacrylate polymer. The equilibrium structure, confirmed by a subsequent vibrational analysis, was found to be very similar to the

structure of the iron(II) sulfate cross-linked polymer. However, for the cadmium complex a less compact structure has been obtained, i.e. the calculated cadmium-nitrogen bond lengths are within 2.320 and 2.334 Å for the central pyridyl-moiety and of 2.395 and 2.405 Å for the terminal pyridyl-moiety. These bonds are significantly longer than the corresponding iron-nitrogen bonds. In addition, the octahedral ligand sphere spanned by the terpyridine shows a pronounced distortion since the terpyridine-cage is undersized for coordination of cadmium(II). Hence, the *bis*terpyridine-cadmium(II) complexes are assumed to be less stable than the *bis*terpyridine-iron(II) complexes, which is reflected in the calculated frequencies of the normal modes of the metal-nitrogen bonds.[58,59] Indeed, the cadmium-nitrogen modes are found in the range of 424 to 575 cm^{-1}, whereas the respective modes of the iron-nitrogen bonds are calculated in the range of 554 and 600 cm^{-1}.

Structural alterations occurring during the self-healing process have been investigated (analogous to the iron(II) sulfate polymer) for the metallopolymer cross-linked by cadmium(II) bromide. For the cadmium(II) bromide polymer, only a slight bathochromic shift of 1.4 cm^{-1} was observed for the Raman band at 1597 cm^{-1} (see Figure 3a) and Figure S2b)), and the studied temperature-dependent evolution of the intensity pattern was found to be fully reversible. The evaluation of the Raman features by means of QM/MM simulations, depicted in Figure 3b), shows a reasonable agreement with experiment, in the region between 1200 and 1800 cm^{-1}. The intensity pattern in this spectral region is dominated by terpyridine modes localized at the *bis*terpyridine-cadmium(II) complex while the vibrational modes of the free terminal ligands are less intense, see Table 2 and Figure S9. Closely related to the findings of the iron(II) metallopolymer discussed in section 4.1.1, the frequencies of the normal modes of the free terpyridine ligand are bathochromically shifted with respect to the corresponding modes of the cadmium(II) complex. This can be seen exemplarily for the simulated band structure at 1670 cm^{-1}, where the modes of the free ligands (1441 and 1453) are calculated at 1658.1 and 1669.2 cm^{-1} and the corresponding modes of the complex (1444 and 1454) are calculated at 1663.7 and 1670.2 cm^{-1}. Similar shifts of, e.g., 4.7 and 5.8 cm^{-1} have been obtained for the simulated Raman band at 1585 cm^{-1}, which is assigned to the experimental band at 1597 cm^{-}

[1] featuring a bathochromic shift of 1.4 cm^{-1} upon heating. This band structure is correlated to several intense modes of the cadmium(II) complex (1381, 1384, 1411, 1412, 1414, 1415, 1420, and 1421) and the four intense modes of the free terpyridine ligands (1406, 1407, 1409, and 1410) found at 1584.9 and 1585.1 cm^{-1}. Hence, the bathochromic shift of 1.4 cm^{-1} observed upon heating for the Raman band at 1597 cm^{-1} can be explained by means of these four intense modes of the free ligand. In addition, all other vibrational modes of the free terpyridine are considerably less intense, which is consistent with the experimental observation that a shift was exclusively observed for this band. Reason for the less pronounced experimental shift, compared to the iron(II) metallopolymer, is provided by the calculated Raman activities (see Table 1 and 2). The intensity of the free ligand is almost identical in both the iron(II) and the cadmium(II) metallopolymers, however, the intensities of the complexated terpyridine ligands are much higher for the *bis*terpyridine-cadmium(II). Accordingly, the measured Raman spectrum of the isolated *bis*terpyridine-cadmium(II) monomer exhibits a band at 1602 cm^{-1}, while the terpyridine monomer features also a band localized at 1602 cm^{-1} (see Figure S8). This finding is consistent with the observation for the metallopolymer, where merely a shift of 1.4 cm^{-1} was found for the Raman band at 1597 cm^{-1}. Analogous to the iron(II) metallopolymer variations of the computational method (XC functional and basis set) lead merely to small deviations of the absolute frequency, however, the relative shifts of the complexated and the free ligands are preserved, see Table S10 and Figures 11 and 12 in the supplementary information.

To exclude a resonance enhancement at the excitation wavelength of 785 nm, the absorption spectrum of the cadmium(II) bromide metallopolymer was simulated. The calculated spectrum, depicted in Figure S12 of the supplementary information, features two absorption bands in the visible range at approximately 650 and 480 nm. Hence, a resonance enhancement seem unlikely at the given excitation wavelength.

4.2 Dissociation of Ionic Clusters

As shown recently by SAXS measurements, the metallopolymers studied form nano structures, which are presumably due to the presence of ionic clusters, where several terpyridine complexes are connected by attractive interactions with anionic counter ions, e.g., sulfate and bromide.[29,30] In order to obtain insight into the intrinsic structure and energies of these ionic clusters, quantum chemical calculations have been performed. Therefore, the size of the model systems for both the iron(II) sulfate and the cadmium(II) bromide cross-linked polymer had to be (at least) doubled, while the two complexes have been placed on top of each other, twisted by 90° and bridged by a counter ion, see Figures 5b) and 6b). To investigate interactions of these bridged complexes, relaxed PES have been calculated along the coordinate *R* describing the distance between one of the complexes and the bridging counter ion. This way a prediction of a thermal dissociation along *R* is obtained. Considering the large size of the model, containing almost 1300 atoms, the MM region was extended to include the polymer backbone as well as the free ligands, which are not involved in the self-healing scheme based on ionic clusters. For describing interactions between the complexes, the QM region was designed to comprise the two metal complexes and all counter ions as depicted in Figure 1e).

4.2.1 Iron(II) cross-linked polymer

In order to study the attractive interactions between the *bis*terpyridine-iron(II) complexes and the sulfate counter ions in the metallopolymer, partial geometry optimizations along the coordinate *R* at the QM/MM level of theory have been carried out using the enhanced polymer model depicted in Figure S1f) of the supporting information. The PES along *R*, illustrated in Figure 5a), was calculated starting from the fully relaxed equilibrium structure at *R* = 5.7 Å, displayed in Figure 5b). From this structure *R* was stepwise decreased / increased yielding the next point of the PES. Two further minima at 3.3 (0.09 eV) and 9.0 Å (0.17 eV) have been obtained, which are separated from the global minimum at 5.7 Å by barriers of 0.24 and 0.37 eV, respectively. The presence of these

three minima is related to the fact that both sulfate counter ions are localized between the *bis*terpyridine-iron(II) complexes, hence, increasing *R* for one sulfate ion leads to an enhanced interaction between the complexes and the other sulfate ion. However, after the minimum at 9.0 Å, where only one sulfate counter ion is bridging the iron(II) complexes (see Figure 5c)), the electronic ground state energy rises rapidly to 0.87 eV at *R* = 15 Å. Increasing *R* further to 30 Å only leads to a slight rise of the ground state energy to 0.95 eV, see structure in Figure 5d). At this geometry the *bis*terpyridine complexes are isolated, while there are still interactions between the polymer backbones. Thus, a further increase of the energy is expected before the two metallopolymers are entirely separated.

SAXS measurements indicated the presence of nano structures, e.g., ionic clusters. This finding is corroborated by the QM/MM simulations on the iron(II) sulfate cross-linked metallopolymer, which also point to the presence of stable ionic clusters. In fact the attractive interactions between the cationic *bis*terpyridine-iron(II) complexes and the sulfate counter ions lead to very stable structures, as shown here for the iron(II) sulfate ionic cluster model. A healing based on the complete dissociation of the clusters can be excluded, because the calculations indicate that in case of the iron(II) metallopolymer energies of almost one eV are necessary for a significant opening of the model clusters, which is not possible at the given temperature of 100 °C.

4.2.2 Cadmium(II) cross-linked polymer

The calculation of the relaxed PES along the coordinate *R* has been repeated for the cadmium(II) metallopolymer. The starting point for the PES shown in Figure 6a) was the fully relaxed equilibrium structure depicted in Figure 6b). In this equilibrium structure, where two bromide ions are attached to each complex, the global minimum of the calculated PES is at $R = 4.9$ Å. A second minimum was found at $R = 4.0$ Å (0.21 eV), where one terpyridine complex bears three bromide ions and the other one only one. These minima are separated by barriers of 0.29 and 0.08 eV, respectively. Enlarging *R* from the global equilibrium structure to about 7 Å leads only to a slight increase of the electronic ground state energy, however, for distances larger than 7 Å the energy increases rapidly and reaches a value of 2.58 eV at 30 Å. Interestingly, the dissociation of the bridged complexes takes place while the attractive interactions of the polymer are still dominant, see Figure 6c).

In addition to the optimized clew conformation of the cadmium metallopolymer shown in Figure 6b), a conformation bearing orthogonally oriented methacrylate moieties has been optimized (see Figure S13b)). Hence, the dissociation energy is exclusively governed by the interactions of the bridged complexes. The PES calculated by means of the optimized metallopolymer features only one minimum at $R = 4.3$ Å, see Figure S13a) of the supplementary information. Analogous to the previously described clew conformation, the region of the PES between 3.8 and 7.0 Å features no significant alterations of the ground state energy. However, further increasing *R* leads to a rapid energy increase. Since dissociation involves in this conformation only the bridged complexes the dissociation energy is already achieved at 15 Å (0.44 eV); and further stretching to 30 Å (0.44 eV, see structure in Figure S13c)) does not affect the ground state energy further.

Due to strong interactions of the *bis*terpyridine-cadmium(II) complex bridged by bromide and of the polymer, a self-healing mechanism based on the opening and subsequent recross-linking of ionic clusters to occur at 100°C appears highly unlikely according to the quantum chemical simulations. This is the case for both the clew conformation, where interactions of the complexes as

well as of the polymer are present, as well as for the orthogonal conformation, where interactions of the complexes are predominant.

5. Conclusions

The thermally induced self-healing mechanism in lauryl methacrylate metallopolymers cross-linked by iron(II) sulfate and cadmium(II) bromide was studied by a joint theoretical-spectroscopic investigation. Experimentally, temperature-dependent Raman spectroscopy was applied to investigate structural alterations during the healing process, whereas reversible bathochromic shifts of Raman bands associated with a structural alteration upon heating have been observed for both metallopolymers. However, Raman spectroscopy alone is unable to provide detailed insight on the thermally induced structural changes of the polymer. In order to investigate these structural alterations and to unravel the underlying self-healing mechanism for this class of metallopolymers on a molecular level, theoretical methods were employed. Hence, QM/MM simulations have been carried out with respect to two scenarios: i) A thermally activated decomplexation of the metal-terpyridine cross-linking and a subsequent new cross-linking upon cooling and ii) an thermally induced cleavage of present ionic clusters formed by several complexes interacting with the negatively charged counter ions, e.g., sulfate and bromide. The existence of ionic clusters for these metallopolymers was deduced from SAXS measurements. However, such measurements do not provide molecular information and energetics with respect to a contribution of such nanostructures to the self-healing properties.

Appropriate QM/MM model systems were constructed, containing one *bis*terpyridine-iron(II) or *bis*terpyridine-cadmium(II) with the respective counter ion (sulfate and bromide) and two free terpyridine ligands linked by a methacrylate based polymer to the central metal complex. The focus was set on the quantum chemical description of the complex and the free ligands by means of DFT applying a functional based on B3LYP containing 15% of exact exchange, while the polymer was described by molecular mechanics. Subsequently, insight into the Raman bands could be obtained by QM/MM simulations of the vibrational frequencies and the Raman scattering intensities. The decent agreement between the theoretical and the experimental intensity pattern, in case of both metallopolymers, is encouraging since it shows that the applied QM/MM models are appropriate to

study cross-linked metallopolymers. The simulations on the iron(II) sulfate as well as the cadmium(II) bromide polymers exhibit a slight bathochromic shift of the vibrational modes of the *bis*terpyridine-metal complex with respect to the free terpyridine ligands indicating a thermally induced decomplexation of the cross-linking complexes. Further simulations on a semi-decomplexated model, where the iron(II) ion is stabilized by merely one terpyridine moiety and the sulfate counter ion, present also bathochromic shifts of the Raman features in the range of the experimentally measured shifts (3 to 4 cm^{-1}). These relative shifts of the analogous metal complex free ligand centered vibrational modes are presumed upon variation of both the XC functional as well as of the basis set and, thus supports the assumption that the healing process is correlated to a decomplexation of the cross-linking complexes. This assumption is supported by Raman measurements on the isolated ligands and metal complexes leading to very similar shifts of the Raman bands in iron(II) terpyridine (6 cm^{-1}) and cadmium(II) bromide (0 cm^{-1}) with respect to the free terpyridine ligand.

The second mechanisms discussed for the self-healing of metallopolymers is based on reversible interactions between the complexes and the anionic counter ions. Thus, extended model systems for both metallopolymers were designed for QM/MM simulations in order to study the properties of such ionic clusters. Of particular interest was the dissociation energy of such ionic clusters since self-healing is observed at 100 °C.

The calculation of relaxed PESs with respect to the cleavage of two complexes bridged by a counter ion (as a model system for theoretical studies on a smallest possible ionic cluster) exhibit two minima, correlated to molecular structures with an imbalanced and an even distribution of the counter ions on the complexes. The global minima with an even distribution of the counter ions between the complexes were found to be energetically very stable: Stretching the complexes up to 30 Å requires an energy of 0.95 and 2.58 eV for the iron(II) sulfate and the cadmium(II) bromide cross-linked polymers, respectively. Hence, a significant thermally induced dissociation of the very stable ionic clusters and a subsequent formation of a new cross-links seems highly unlikely at

temperatures of about 100°C (approximately 0.03 eV) based on the results of the quantum chemical study. Thus, the applied quantum chemical simulations and Raman spectra of the metallopolymers and the monomers point to a self-healing mechanism based on a reversible thermal decomplexation of the *bis*terpyridine metal complexes.

Acknowledgements

This research was supported financially by the Deutsche Forschungsgemeinschaft within the framework of the SPP 1568 “Design and Generic Principles of Self-healing Materials”. J. G. is grateful to the 7th Framework Programme of the European Union. S.B. is grateful to the Fonds der Chemischen Industrie (FCI) for a generous Ph.D. stipend. All calculations have been performed at the Universitätsrechenzentrum of the FriedrichSchiller University of Jena and the HP computers of the Theoretical Chemistry group of Jena.

References

1. X. Chen, M. A. Dam, K. Ono, A. Mal, H. Shen, S. R. Nutt, K. Sheran, and F. Wudl, *Science*, 2002, **295**, 1698–1702.
2. R. P. Wool, *Soft Matter*, 2008, **4**, 400–418.
3. Y. Yang and M. W. Urban, *Chem. Soc. Rev.*, 2013, **42**, 7446–7467.
4. M. D. Hager, P. Greil, C. Leyens, S. van der Zwaag, and U. S. Schubert, *Adv. Mater.*, 2010, **22**, 5424–5430.
5. N. K. Guimard, K. K. Oehlenschlaeger, J. Zhou, S. Hilf, F. G. Schmidt, and C. Barner-Kowollik, *Macromol. Chem. Phys.*, 2012, **213**, 131–143.
6. S. Billiet, X. K. D. Hillewaere, R. F. A. Teixeira, and F. E. Du Prez, *Macromol. Rapid Commun.*, 2013, **34**, 290–309.
7. M. Q. Zhang and M. Z. Rong, *Polym. Chem.*, 2013, **4**, 4878–4884.
8. F. Herbst, D. Döhler, P. Michael, and W. H. Binder, *Macromol. Rapid Commun.*, 2013, **34**, 203–220.
9. M. Samadzadeh, S. H. Boura, M. Peikari, S. M. Kasiriha, and A. Ashrafi, *Prog. Org. Coat.*, 2010, **68**, 159–164.
10. S. J. García, H. R. Fischer, and S. van der Zwaag, *Prog. Org. Coat.*, 2011, **72**, 211 – 221.
11. Á. García, E. Schlangen, M. van de Ven, and G. van Bochove, *Const. Build. Mater.*, 2012, **30**, 59 – 65.
12. Á. García, *Fuel*, 2012, **93**, 264 – 272.
13. J. E. Gray and B. Luan, *J. Alloys and Compd.*, 2002, **336**, 88 – 113.
14. X. Chen, F. Wudl, A. K. Mal, H. B. Shen, and S. R. Nutt, *Macromolecules*, 2003, **36**, 1802–1807.
15. J. Kötteritzsch, S. Stumpf, S. Hoeppener, J. Vitz, M. D. Hager, and U. S. Schubert, *Macromol. Chem. Phys.*, 2013, **214**, 1636–1649.
16. U. Lafont, H. van Zeijl, and S. van der Zwaag, *Appl. Mat. Interfaces*, 2012, **4**, 6280–6288.
17. Y. Amamoto, H. Otsuka, A. Takahara, and K. Matyjaszewski, *Adv. Mater.*, 2012, **24**, 3975–3980.
18. P. Cordier, F. Tournilhac, C. Soulie-Ziakovic, and L. Leibler, *Nature*, 2008, **451**, 977–980.
19. D. Montarnal, P. Cordier, C. Soulie-Ziakovic, F. Tournilhac, and L. Leibler, *J. Polym. Sci., Part A: Polym. Chem*, 2008, **46**, 7925–7936.
20. L. R. Hart, J. L. Harries, B. W. Greenland, H. M. Colquhoun, and W. Hayes, *Polym. Chem.*, 2013, **4**, 4860–4870.
21. F. Herbst, S. Seiffert, and W. H. Binder, *Polym. Chem.*, 2012, **3**, 3084–3092.
22. S. J. Kalista and T. C. Ward, *J. R. Soc. Interface*, 2007, **4**, 405–411.
23. S. J. Kalista, J. R. Pflug, and R. J. Varley, *Polym. Chem.*, 2013, **4**, 4910–4926.
24. S. Burattini, H. M. Colquhoun, D. Fox, D. Friedmann, B. W. Greenland, P. J. F. Harris, W. Hayes, M. E. Mackay, and S. J. Rowan, *Chem. Commun.*, 2009, 6717–6719.
25. S. Burattini, H. M. Colquhoun, B. W. Greenland, and W. Hayes, *Faraday Discuss.*, 2009, **143**, 251–264.
26. M. Zhang, D. Xu, X. Yan, J. Chen, S. Dong, B. Zheng, and F. Huang, *Angew. Chem. Int. Ed.*, 2012, **51**, 7011–7015.
27. B. Zheng and F. Huang, *Chem. Soc. Rev.*, 2012, **41**, 6042–6065.
28. M. Burnworth, L. Tang, J. R. Kumpfer, A. J. Duncan, F. L. Beyer, G. L. Fiore, S. J. Rowan, and C. Weder, *Nature*, 2011, **472**, 334–337.
29. S. Bode, L. Zedler, F. H. Schacher, B. Dietzek, M. Schmitt, J. Popp, M. D. Hager, and U. S. Schubert, *Adv. Mater.*, 2013, **25**, 1634–1638.
30. S. Bode, R. K. Bose, S. Matthes, M. Ehrhardt, A. Seifert, F. H. Schacher, R. M. Paulus, S. Stumpf, B. Sandmann, J. Vitz, A. Winter, S. Hoeppener, S. J. Garcia, S. Spange, S. van der Zwaag, M. D. Hager, and U. S. Schubert, *Polym. Chem.*, 2013, **4**, 4966–4973.
31. E. Carrington and J. M. Gosline, *J. Am. Malacol. Bull.*, 2004, 135–142.
32. C. Sun and J. H. Waite, *J. Biol. Chem.*, 2005, **280**, 39332–39336.
33. M. J. Harrington, A. Masic, N. Holten-Andersen, J. H. Waite, and P. Fratzl, *Science*, 2010, **328**, 216–220.

34. L. Zedler, M. D. Hager, U. S. Schubert, M. J. Harrington, M. Schmitt, J. Popp, and B. Dietzek, *Mater. Today*.
35. S. Vasiliu, B. Kampe, F. Theil, B. Dietzek, D. Döhler, P. Michael, W. H. Binder, and J. Popp, *Appl. Spectrosc.*
36. B. Chu and B. S. Hsiao, *Chem. Rev.*, 2001, **101**, 1727–1762.
37. R. J. Varley and S. van der Zwaag, *Polym. Test.*, 2008, **27**, 11 – 19.
38. R. J. Varley and S. van der Zwaag, *Polym. Int.*, 2010, **59**, 1031–1038.
39. R. J. Varley, S. Shen, and S. van der Zwaag, *Polymer*, 2010, **51**, 679 – 686.
40. R. J. Varley and S. van der Zwaag, *Acta Mater.*, 2008, **56**, 5737 – 5750.
41. S. Dapprich, I. Komáromi, K. S. Byun, K. Morokuma, and M. J. Frisch, *J. Mol. Struct. (Theochem)*, 1999, **462**, 1 – 21.
42. T. Vreven, K. S. Byun, I. Komáromi, S. Dapprich, J. A. Montgomery, K. Morokuma, and M. J. M. J. Frisch, *J. Chem. Theory Comput.*, 2006, **2**, 815–826.
43. M. D. Chipara, M. Chipara, E. Shansky, and J. M. Zaleski, *Polym. Adv. Technol.*, 2009, **20**, 427–431.
44. N. Holten-Andersen, M. J. Harrington, H. Birkedal, B. P. Lee, P. B. Messersmith, K. Y. C. Lee, and J. H. Waite, *Proc. Natl. Acad. Sci.*, 2011, 1–5.
45. M. J. Frisch, G. W. Trucks, H. B. Schlegel, G. E. Scuseria, M. A. Robb, J. R. Cheeseman, G. Scalmani, V. Barone, B. Mennucci, G. A. Petersson, H. Nakatsuji, M. Caricato, X. Li, H. P. Hratchian, A. F. Izmaylov, G. Z. J. Bloino, J. L. Sonnenberg, M. Hada, M. Ehara, K. Toyota, R. Fukuda, J. Hasegawa, M. Ishida, T. Nakajima, Y. Honda, O. Kitao, H. Nakai, T. Vreven, J. J. A. Montgomery, J. E. Peralta, F. Ogliaro, M. Bearpark, J. J. Heyd, E. Brothers, K. N. Kudin, V. N. Staroverov, R. Kobayashi, J. Normand, K. Raghavachari, A. Rendell, J. C. Burant, S. S. Iyengar, J. Tomasi, M. Cossi, N. Rega, J. M. Millam, M. Klene, J. E. Knox, J. B. Cross, V. Bakken, C. Adamo, J. Jaramillo, R. Gomperts, R. E. Stratmann, A. J. A. O. Yazyev, C. P. R. Cammi, J. W. Ochterski, R. L. Martin, K. Morokuma, V. G. Zakrzewski, G. A. Voth, P. Salvador, J. J. Dannenberg, S. Dapprich, A. D. Daniels, O. Farkas, J. B. Foresman, J. V. Ortiz, J. Cioslowski, and D. J. Fox, *Gaussian 09, Revision A.1*, Gaussian 09, Revision A.1, Gaussian, Inc., Wallingford, CT, 2009.
46. M. Reiher, O. Salomon, and B. Artur Hess, *Theor. Chem. Acc.*, 2001, **107**, 48–55.
47. O. Salomon, M. Reiher, and B. A. Hess, *J. Chem. Phys.*, 2002, **117**, 4729–4737.
48. A. D. Becke, *J. Chem. Phys.*, 1993, **98**, 5648–5652.
49. C. Lee, W. Yang, and R. G. Parr, *Phys. Rev. B*, 1988, **37**, 785–789.
50. M. Dolg, U. Wedig, H. Stoll, and H. Preuss, *J. Chem. Phys.*, 1987, **86**, 2123–2131.
51. P. C. Hariharan and J. A. Pople, *Theor. Chim. Acta*, 1973, **28**, 213–222.
52. R. J. Davidson, E. W. Ainscough, A. M. Brodie, G. B. Jameson, M. R. Waterland, H. R. Allcock, M. D. Hindenlang, B. Moubaraki, K. S. Murray, K. C. Gordon, R. Horvath, and G. N. L. Jameson, *Inorg. Chem.*, 2012, **51**, 8307–8316.
53. J. P. Merrick, D. Moran, and L. Radom, *J. Phys. Chem.*, 2007, **111**, 11683–11700.
54. J. Tomasi, B. Mennucci, and R. Cammi, *Chem. Rev.*, 2005, **105**, 2999–3093.
55. M. Wächtler, J. Guthmuller, L. González, and B. Dietzek, *Coord. Chem. Rev.*, 2012, **256**, 1479 – 1508.
56. S. Kupfer, M. Wächtler, J. Guthmuller, J. Popp, B. Dietzek, and L. González, *J. Phys. Chem. C*, 2012, **116**, 19968–19977.
57. S. Kupfer, J. Guthmuller, and L. González, *J. Chem. Theory Comput.*, 2013, **9**, 543–554.
58. H. R. Holyer, C. D. Hubbard, S. F. A. Kettle, and R. G. Wilkins, *Inorg. Chem.*, 1965, **5**, 622–625.
59. M. A. R. Meier, B. G. G. Lohmeijer, and U. S. Schubert, *J. Mass Spectrom.*, 2003, **38**, 510–516.
60. M. Halls, J. Velkovski, and H. Schlegel, *Theor Chem Acc*, 2001, **105**, 413–421.

Figure 1

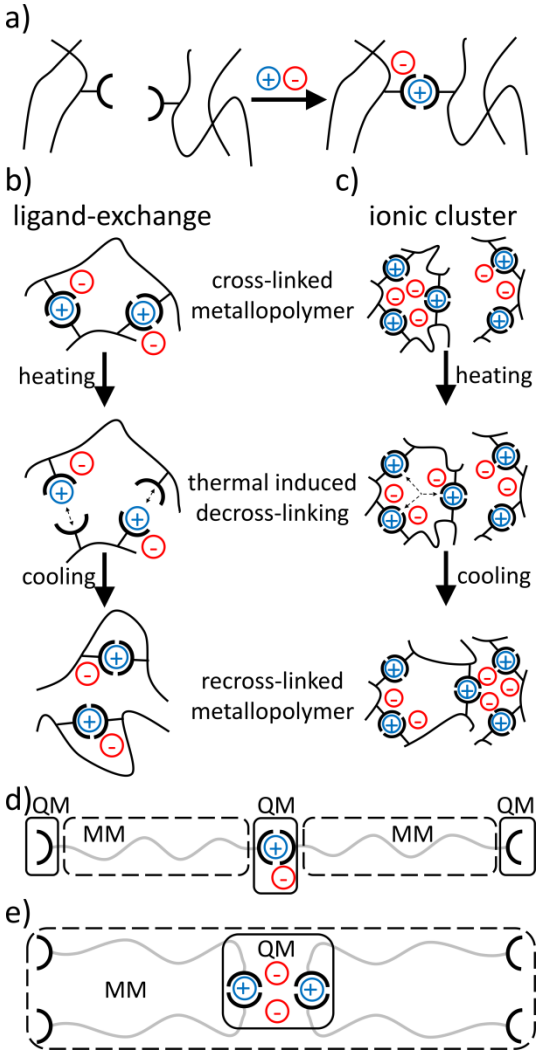

Schematic representation of the reversible cross-linking process in metallopolymers. a) depicts the cross-linking using metal salts. b) and c) illustrate the thermally induced self-healing process based on a decomplexation of the complexes (ligand-exchange; b)) and by means of the disscociation of ionic clusters, followed by a reorganization (c)). QM/MM model systems to obtain insight into the proposed healing mechanisms are shown in d) for the ligand-exchange and in e) for ionic clusters.

Figure 2

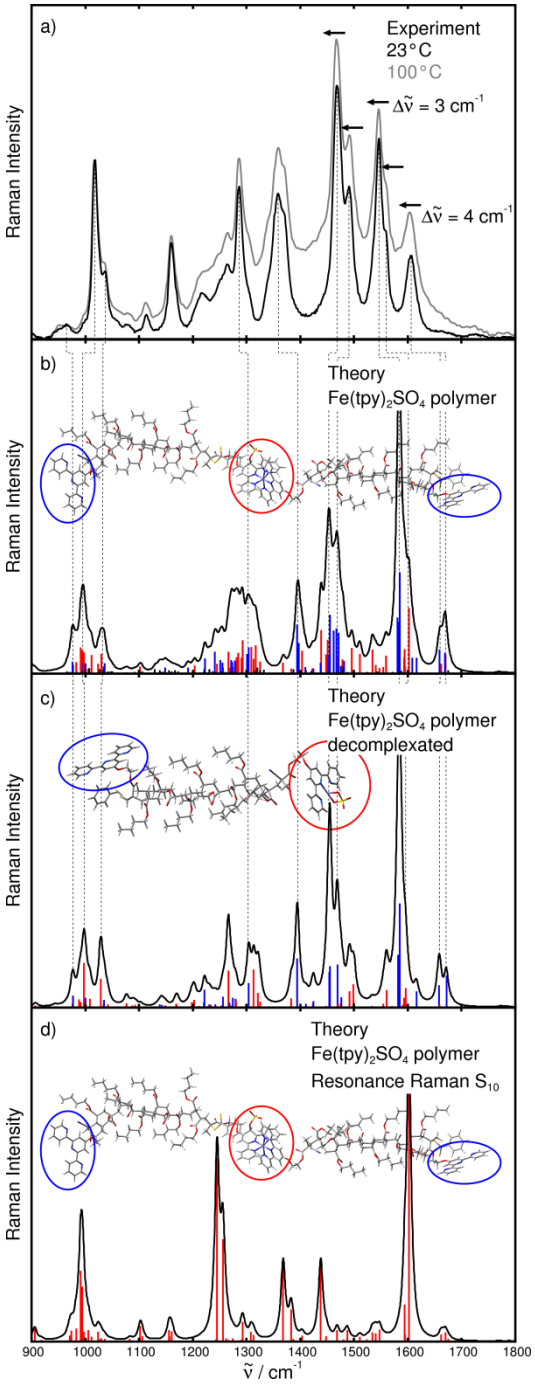

Raman spectra of the iron(II) sulfate metallopolymer. a) depicts temperature-dependent Raman spectra at 23 and 100 °C along with the thermally induced bathochromic shifts of the intensity pattern. b) and c) display calculated Raman spectra at the QM/MM level of theory using B3LYP(15) with the 6-31G(d) basis set and the universal force field for two polymer models. Vibrational modes centered at the *bis*terpyridine-iron(II) complex are shown in red and modes of the free terminal terpyridine moieties are shown in blue. d) features the simulated RR spectrum

calculated at an excitation wavelength of 647 nm using the excited state gradients, transition dipole moment and excitation energy of the S_{10} state.

Figure 3

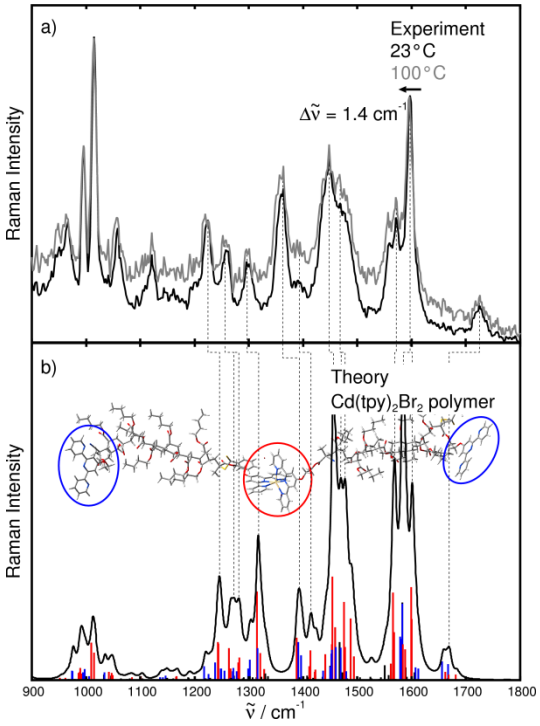

Raman spectra of the cadmium(II) bromide metallopolymer. a) depicts temperature-dependent Raman spectra at 23 and 100 °C along with the thermally induced bathochromic shift of the intensity pattern, b) displays calculated Raman spectrum at the QM/MM level of theory using B3LYP(15) with the 6-31G(d) basis set and the universal force field for the polymer model. Vibrational modes centered at the *bis*terpyridine-cadmium(II) complex are shown in red and modes of the free terminal terpyridine moieties are shown in blue.

Figure 4

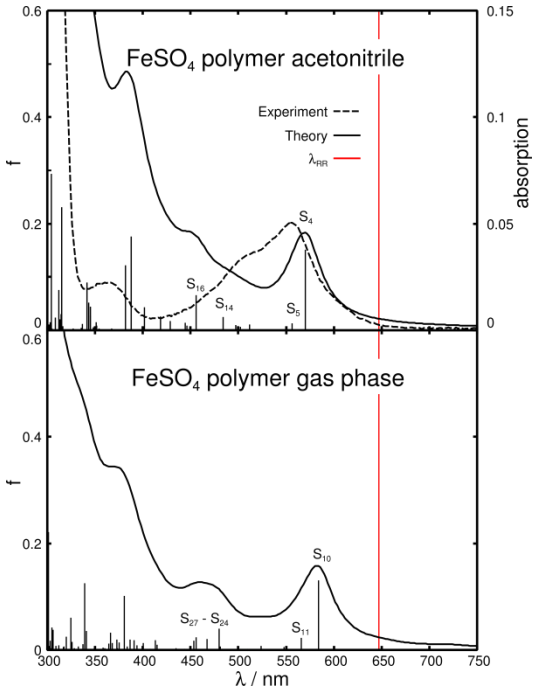

Absorption spectra of the iron(II) sulfate metallopolymer. a) shows the experimental and simulated UV-vis spectra in acetonitrile, the simulations were performed at the QM/MM level of theory using B3LYP(15) with the 6-31G(d) basis set and the universal force field. b) depicts the simulated absorption in gas phase. The red line corresponds to the applied excitation wavelength of the Raman measurements.

Figure 5

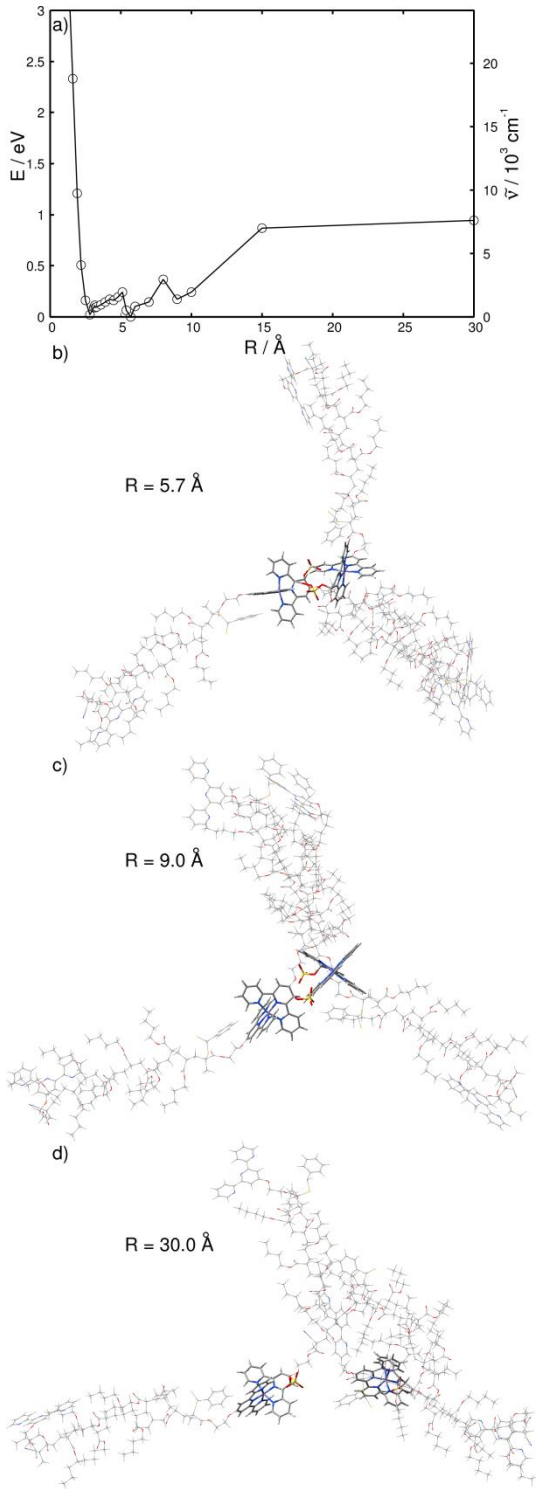

Panel a) depicts the calculated relaxed PES of the iron(II) sulfate metallopolymer at the QM/MM level of theory using B3LYP(15) with the 6-31G(d) basis set and the universal force field with respect to the distance *R* (between one complex and the bridging counter ion) describing the cleavage of the ionic cluster up to *R* = 30 Å. b), c) and d) depict the global minimum of the PES

(R = 5.7 Å), the local minimum at R = 9.0 Å, and the opened cluster at R = 30 Å.

Figure 6

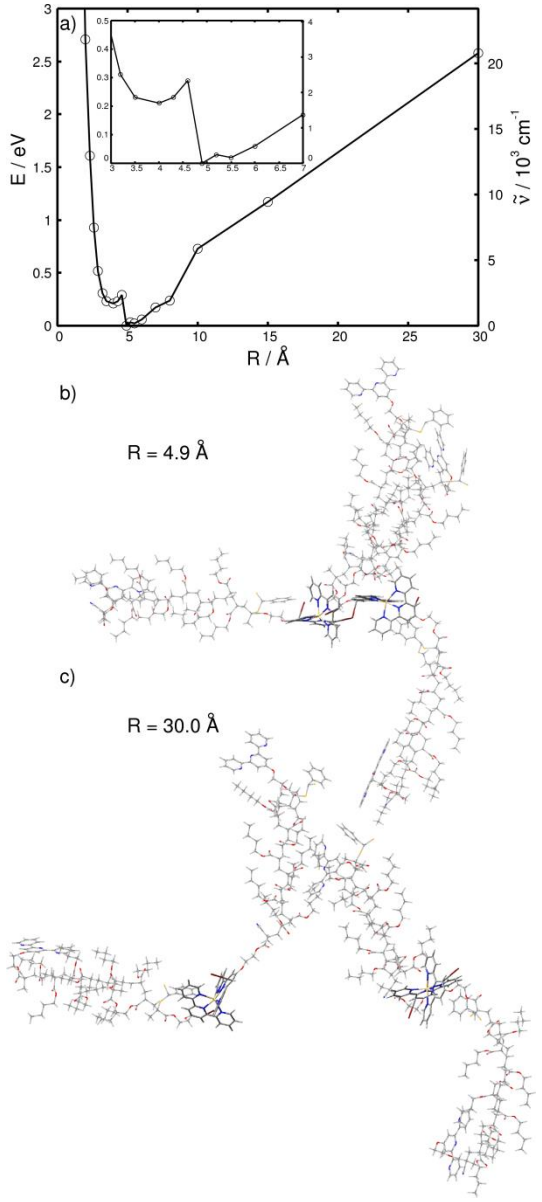

Panel a) depicts the calculated relaxed PES of the cadmium(II) bromide metallopolymer at the QM/MM level of theory using B3LYP(15) with the 6-31G(d) basis set and the universal force field with respect to the distance *R* (between one complex and the bridging counter ion) describing the cleavage of the ionic cluster up to *R* = 30 Å. b) and c) depicts the global minimum of the PES (*R* = 4.9 Å) and the opened cluster at *R* = 30 Å.

Table 1

		iron(II) sulfate metallopolymer		iron(II) sulfate semi-decomplexed metallopolymer		
assignment	mode	$\tilde{\nu}$/ cm^{-1}	I / Å^{4}amu^{-1}	mode	$\tilde{\nu}$/ cm^{-1}	I / Å^{4}amu^{-1}
free tpy asym	1415	1581.3	335	716	1581.8	305
free tpy asym	1416	1581.7	309	-	-	-
free tpy sym	1417	1584.9	593	717	1585.0	602
free tpy sym	1418	1585.0	605	-	-	-
complex tpy asym	1422	1593.5	94	720	1592.9	57
complex tpy asym	1424	1594.5	200	-	-	-
complex tpy sym	1425	1595.3	42	721	1595.9	113
complex tpy sym	1428	1602.3	394	-	-	-
free tpy sym	1450	1658.7	144	733	1658.3	127
complex tpy sym	1452	1661.7	58	-	-	-
free tpy sym	1461	1668.7	123	-	-	-
complex tpy sym	1462	1669.7	65	739	1671.7	185
complex tpy sym	1463	1670.6	113	-	-	-

Assignment of the calculated vibrational frequencies (cm^{-1}) and relative Raman activities ($Å^4amu^{-1}$) for the iron(II) sulfate cross-linked metallopolymer as well as its semi-decomplexated form.

Table 2

cadmium(II) bromide metallopolymer			
assignment	mode	$\tilde{\nu}$/ cm^{-1}	I / Å^{4}amu^{-1}
complex tpy sym	1381	1568.0	668
complex tpy sym	1384	1569.2	366
free tpy asym	1406	1581.3	333
free tpy asym	1407	1581.7	318
free tpy sym	1409	1584.9	593
free tpy sym	1410	1585.1	586
complex tpy asym	1411	1586.0	60
complex tpy asym	1412	1586.3	274
complex tpy sym	1414	1590.5	235
complex tpy sym	1415	1591.0	99
complex tpy asym	1420	1600.9	701
complex tpy asym	1421	1602.1	469
free tpy asym	1423	1608.7	96
free tpy asym	1426	1614.3	89
free tpy sym	1441	1658.1	143
complex tpy sym	1444	1663.6	62
free tpy sym	1453	1669.2	123
complex tpy sym	1454	1670.2	41

Assignment of the calculated vibrational frequencies (cm^{-1}) and relative Raman activities (Å^{4}amu^{-1}) for the iron(II) sulfate cross-linked metallopolymer as well as its semi-decomplexed form.

Self-healing Mechanism of Metallopolymers investigated by QM/MM Simulations and Raman Spectroscopy

Stephan Kupfer[1,2,§], Linda Zedler[1,2,§], Julien Guthmuller[3], Stefan Bode[4,5], Martin D. Hager[4,5], Ulrich S. Schubert[4,5], Jürgen Popp[1,2,6], Stefanie Gräfe[1,2], Benjamin Dietzek[1,2,6*]

[1]*Institute for Physical Chemistry, Friedrich Schiller University Jena, Helmholtzweg 4, 07743, Jena, Germany*

[2]*Abbe Center of Photonics, Friedrich Schiller University Jena*

[3]*Faculty of Applied Physics and Mathematics, Gdansk University of Technology, Narutowicza 11/12, 80233 Gdansk, Poland*

[4]*Laboratory for Organic and Macromolecular Chemistry, Friedrich Schiller University Jena, Humboldstr. 10, 07743, Jena, Germany*

[5]*Jena Center of Soft Matter, Friedrich Schiller University Jena, Philosophenweg 7, 07743, Jena, Germany*

[6]*Institute for Photonic Technology (IPHT) Jena, Albert-Einstein-Str. 9, 07745, Jena, Germany*

Experimental Section

All used chemicals were purchased from Aldrich, ABCR and Hetcat. They were used without further purification. DMSO was dried with activated mol sieves. Elemental analyses were carried out on a Vario EL III (Elementar) elemental analyzer.

^{1}H and ^{13}C NMR spectra were recorded on a Bruker AC 250 (250 MHz) at 298 K. Chemical shifts are reported in parts per million (ppm, δ scale) relative to the residual signal of the solvent. Coupling constants are given in Hz.

6-(2,2':6',2"-Terpyridin-4'-yloxy)-hexan-1-ol (**1**) was prepared according to literature.[1]

Conversion of 1 with iron(II) sulfate

338 mg (0.97 mmol) of **1** were dissolved in 40 mL methanol. Subsequently, 135 mg iron(II) sulfate heptahydrate (0.49 mmol) were added and the color changed to dark violet. The reaction mixture was stirred for further 18 hours. Afterwards the solvent was evaporated and the residue was washed with 200 mL diethyl ether.

^{1}H NMR (250 MHz, CD_3OD): δ = 1.55 – 2.28 (m, 8H), 3.65 (t, J = 6 Hz, 2H), 4.70 (t, J = 6 Hz, 2H), 7.19 (m, 4H), 7.95 (t, J = 7.25 Hz, 2H), 8.70 (m, 4H) ppm.
^{13}C NMR (62.5 MHz, CD_3OD): δ = 25.3, 25.7, 28.7, 32.2, 61.5, 70.3, 111.2, 123.6, 127.1, 138.5, 152.7, 158.3, 160.8, 168.4 ppm.
Anal. calcd. for $C_{42}H_{46}N_6O_8SFe$: C 59.79, H 5.45, N 9.88, S 3.77; found: C 59.40, H 5.59, N 9.99, S 3.72

Conversion of 1 with cadmium(II) bromide

297 mg (0.85 mmol) of **1** were dissolved in 40 mL methanol. Subsequently, 147 mg cadmium(II) bromide tetrahydrate (0.43 mmol) were added and a precipitate formed. The reaction mixture was stirred for further 18 hours. Afterwards the product was obtained by filtration and was washed with 300 mL diethyl ether.

^{1}H NMR and ^{13}C NMR were not measure due to the bad solubility of the product in all common solvents.
Anal. calcd. for $C_{42}H_{46}N_6O_4Br_2Cd$: C 51.95, H 4.77, N 8.65, Br 16.46; found: C 51.95, H 4.75, N 8.80, Br 16.86

References

[1] U. S. Schubert, C. Eschbaumer, O. Hien, P. R. Andres, *Tetrahedron Lett.* **2001**, *42*, 4705–4707.

Figure S1

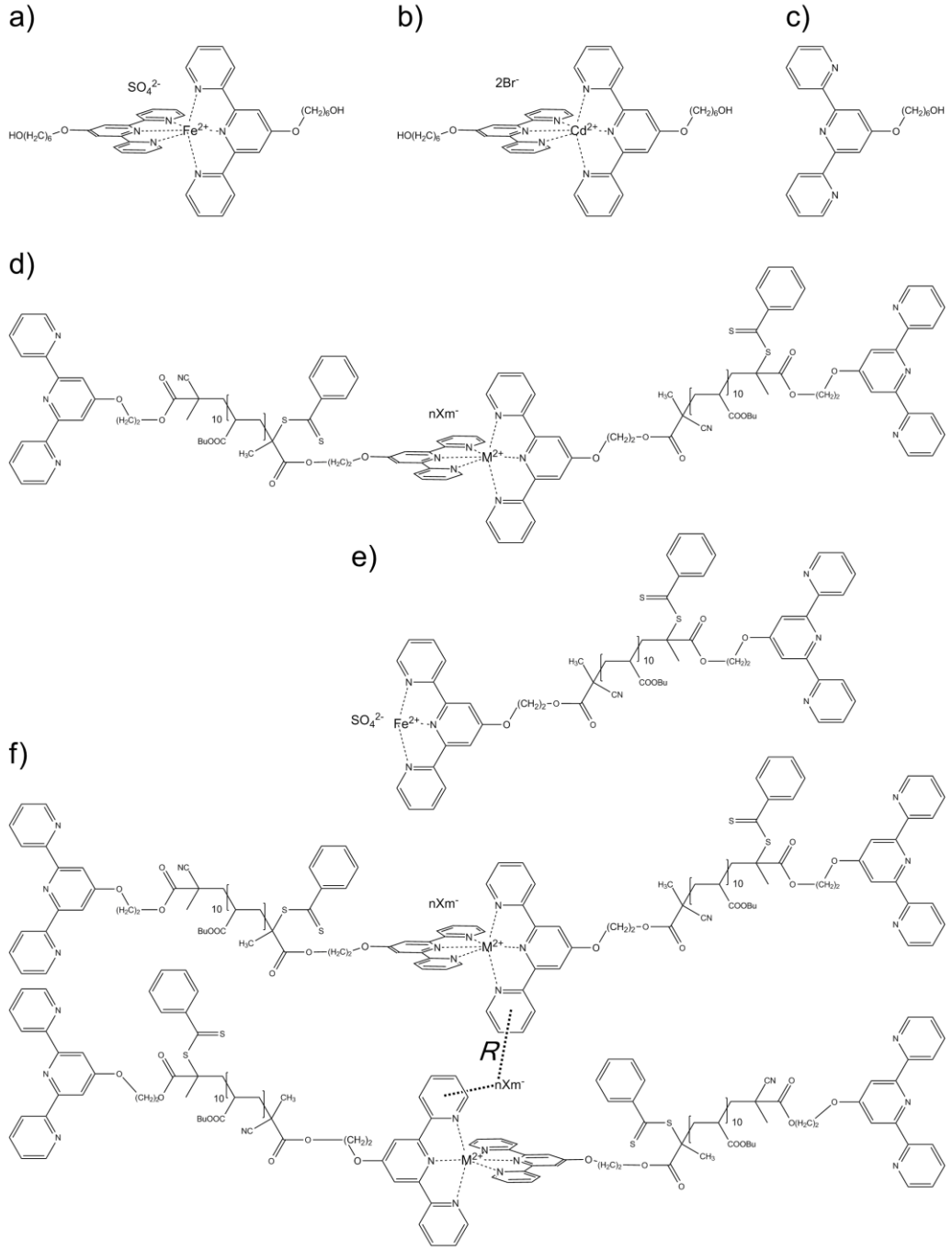

Schematic representation of the iron(II) terpyridine sulfate complex (a)), the cadmium(II) terpyridine bromide complex (b)), and the free terpyridine ligand (c)). d) depict the model systems used for the simulation of the Raman spectra of the iron(II) sulfate and the cadmium(II) bromide cross-linked metallopolymers, and e) the semi-decomplexed metallopolymer. The polymer model used in the calculation of the ionic clusters is illustrated in f); frozen coordinate *R* is indicated.

Figure S2

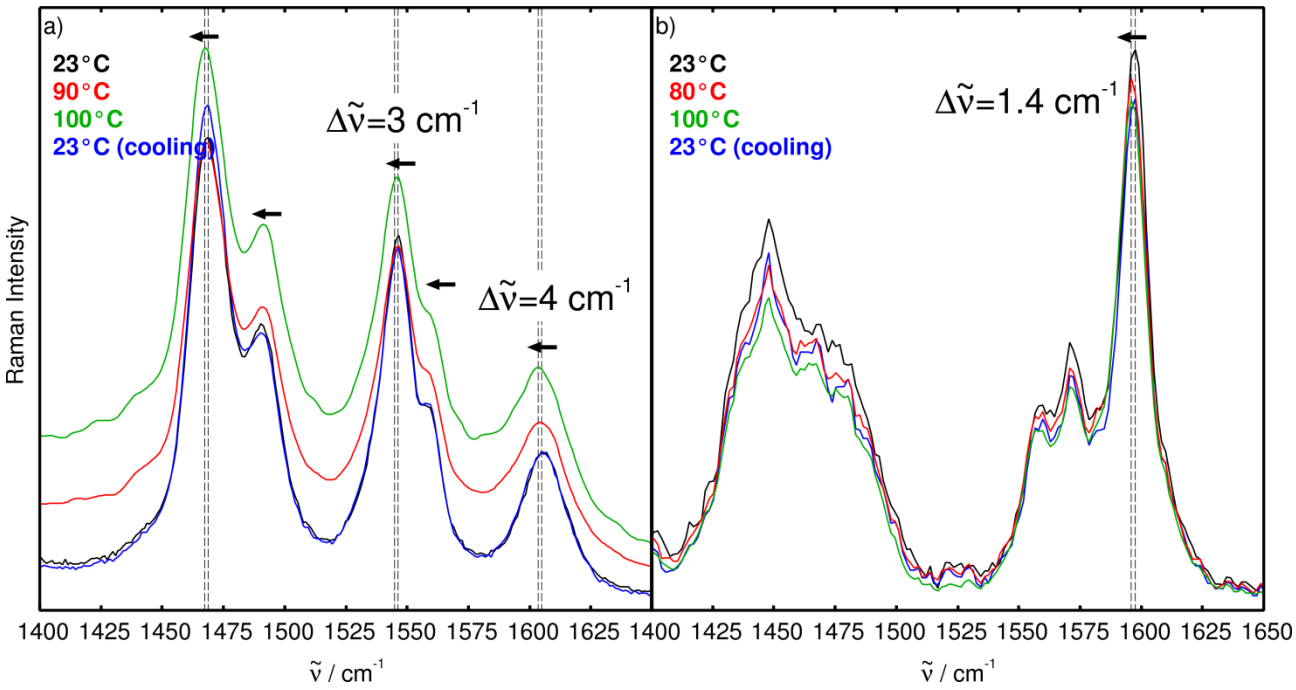

Temperature-dependent Raman spectra of the iron(II) sulfate (a)) and cadmium(II) bromide (b)) cross-linked metallopolymers in the spectral range between 1400 and 1650 cm^{-1}. Vertical dashed lines indicate the observed fully reversible bathochromic shifts of approximately 3 and 4 and 1.4 cm^{-1}.

Figure S3

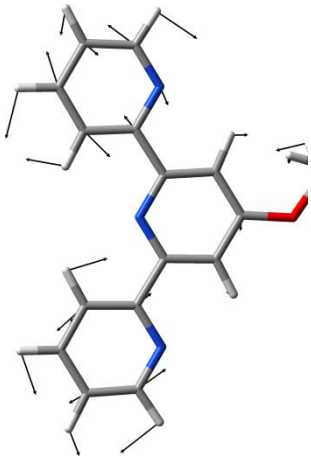

1415

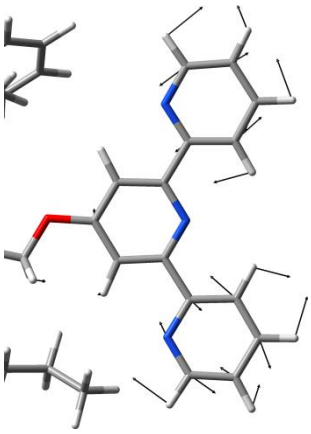

mode 1416

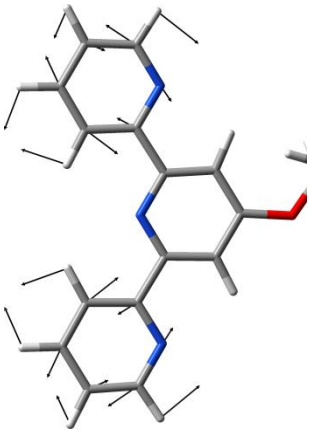

mode 1417

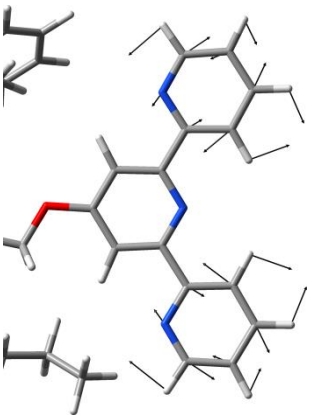

mode 1418

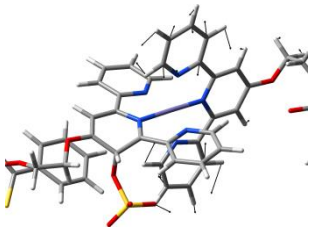

mode 1422

mode 1424

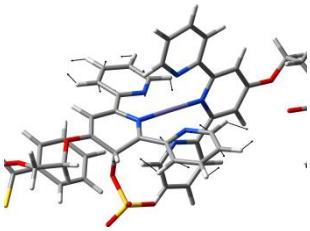

mode 1425

mode 1428

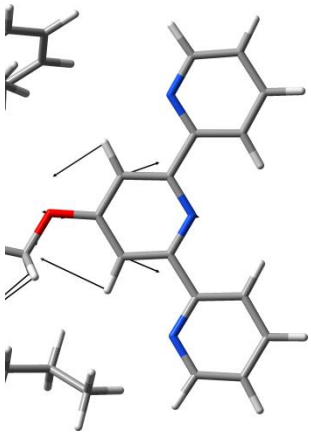

mode 1450

mode 1452

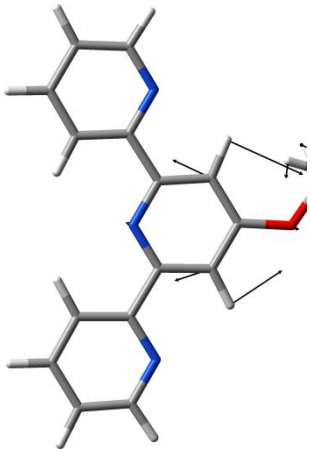

mode 1461

mode 1462

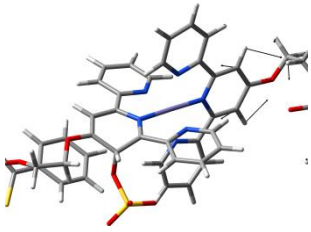

mode 1463

Intense vibrational modes of the iron(II) sulfate metallopolymer contributing to the experimental Raman bands at 1546, 1558, and 1606 cm^{-1}.

Figure S4

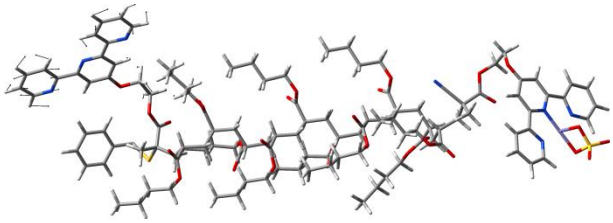

mode 716

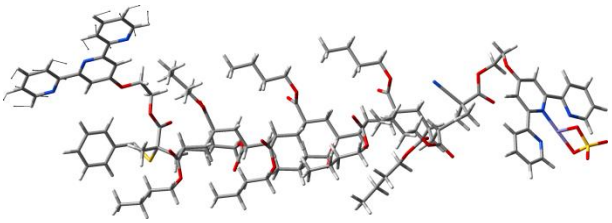

mode 717

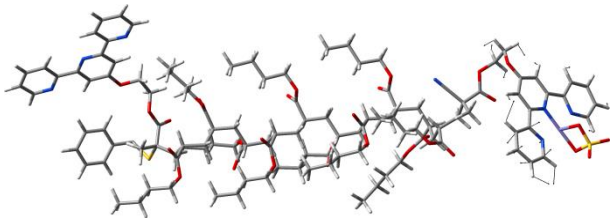

mode 720

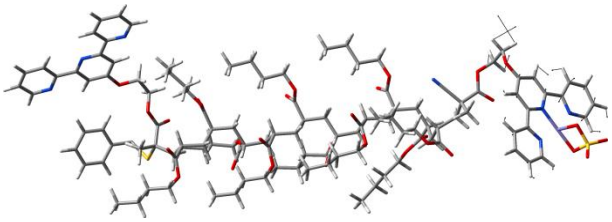

mode 721

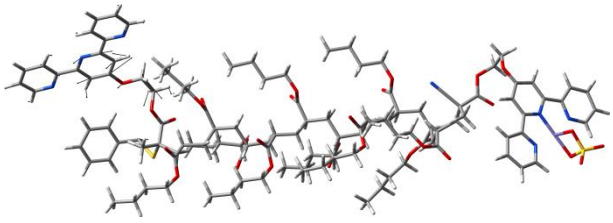

mode 725

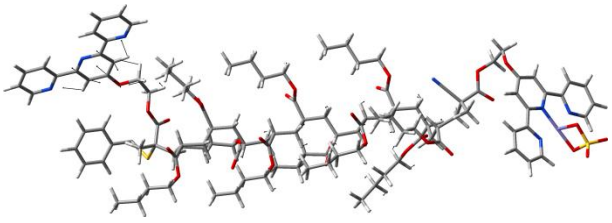

mode 733

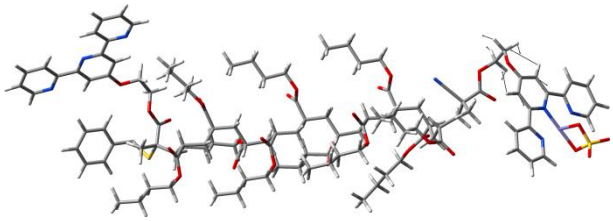

mode 739

Intense vibrational modes of the semi-decomplexed iron(II) sulfate metallopolymer.

Table S5

iron(II) sulfate metallopolymer									
	B3LYP(15)/6-31G(d)			B3LYP(15)/6-311G(d)			B3LYP/6-31G(d)		
assignment	mode	$\tilde{\nu}$/ cm^{-1}	I / Å^{4}amu^{-1}	mode	$\tilde{\nu}$/ cm^{-1}	I / Å^{4}amu^{-1}	mode	$\tilde{\nu}$/ cm^{-1}	I / Å^{4}amu^{-1}
free tpy asym	1415	1581.3	335	1415	1569.3	294	1417	1593.8	340
free tpy asym	1416	1581.7	309	1416	1569.6	212	1418	1594.2	312
free tpy sym	1417	1584.9	593	1417	1572.6	557	1421	1597.5	550
free tpy sym	1418	1585.0	605	1418	1572.8	610	1422	1597.6	572
complex tpy asym	1422	1593.5	94	1422	1583.2	210	1426	1606.1	114
complex tpy asym	1424	1594.5	200	1424	1583.8	87	1427	1607.8	217
complex tpy sym	1425	1595.3	42	1425	1587.9	70	1428	1608.1	43
complex tpy sym	1428	1602.3	394	1428	1591.1	385	1432	1615.0	458
free tpy sym	1450	1658.7	144	1445	1650.5	147	1460	1668.2	138
complex tpy sym	1452	1661.7	58	1447	1654.1	137	1462	1678.1	124
free tpy sym	1461	1668.7	123	1453	1660.8	129	1464	1679.8	111
complex tpy sym	1462	1669.7	65	-	-	-	1466	1681.1	39
complex tpy sym	1463	1670.6	113	1455	1662.9	107	1468	1683.8	36
iron(II) sulfate semi-decomplexed metallopolymer									
	B3LYP(15)/6-31G(d)			B3LYP(15)/6-311G(d)			B3LYP/6-31G(d)		
assignment	mode	$\tilde{\nu}$/ cm^{-1}	I / Å^{4}amu^{-1}	mode	$\tilde{\nu}$/ cm^{-1}	I / Å^{4}amu^{-1}	mode	$\tilde{\nu}$/ cm^{-1}	I / Å^{4}amu^{-1}
free tpy asym	716	1581.8	305	707	1570.0	209	717	1594.3	312
free tpy sym	717	1585.0	602	710	1572.8	606	718	1597.7	569
complex tpy asym	720	1592.9	57	718	1583.0	65	721	1605.9	86
complex tpy sym	721	1595.9	113	719	1584.0	63	723	1608.1	65
free tpy sym	733	1658.3	127	730	1650.2	147	738	1668.1	141
complex tpy sym	739	1671.7	185	736	1664.0	177	740	1681.8	124

Assignment and comparison of the calculated vibrational frequencies (cm^{-1}) and relative Raman activities (Å^{4}amu^{-1}) for the iron(II) sulfate cross-linked metallopolymer as well as its semi-decomplexated form obtained at the B3LYP15/6-31G(d), B3LYP15/6-311G(d), and B3LYP/6-31G(d) levels of theory.

Figure S6

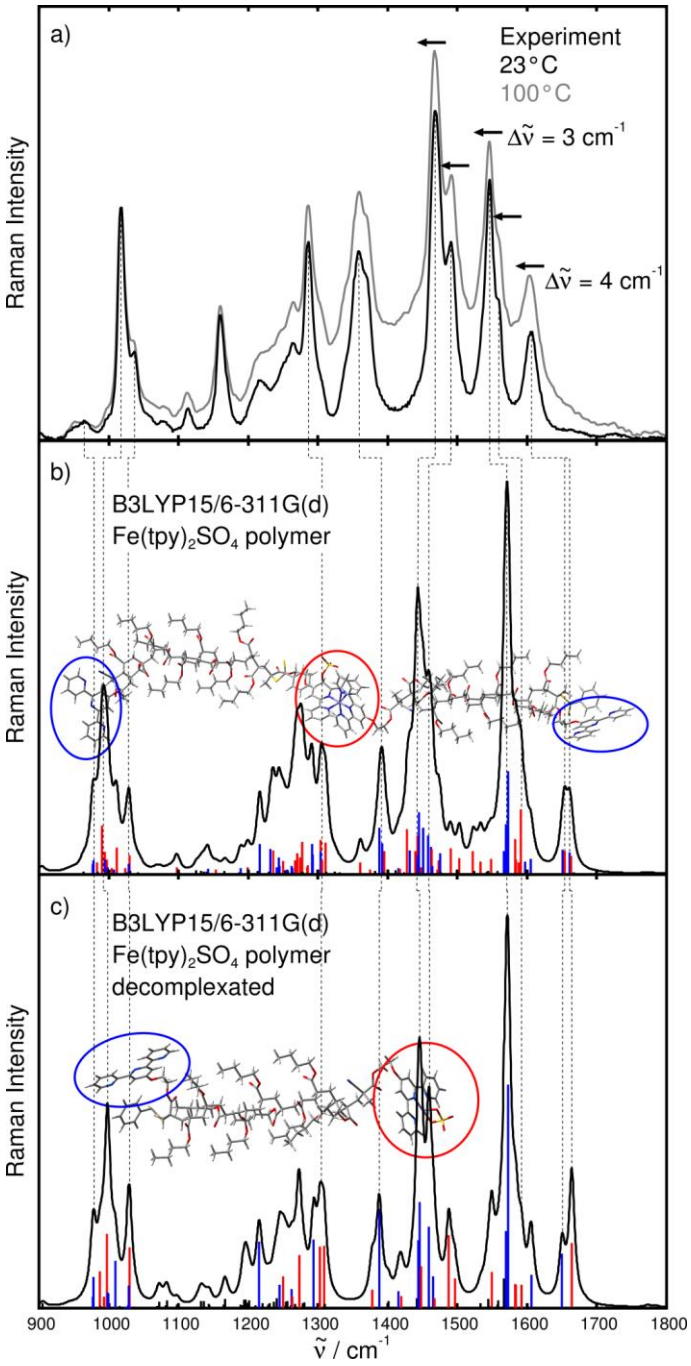

Raman spectra of the iron(II) sulfate metallopolymer. a) depicts temperature-dependent Raman spectra at 23 and 100 °C along with the thermally induced bathochromic shifts of the intensity pattern. b) and c) display calculated Raman spectra at the QM/MM level of theory using B3LYP(15) and the 6-311G(d) basis set and the universal force field for two polymer models. Vibrational modes centered at the *bis*terpyridine-iron(II) complex are shown in red and modes of the free terminal terpyridine moieties are shown in blue.

Figure S7

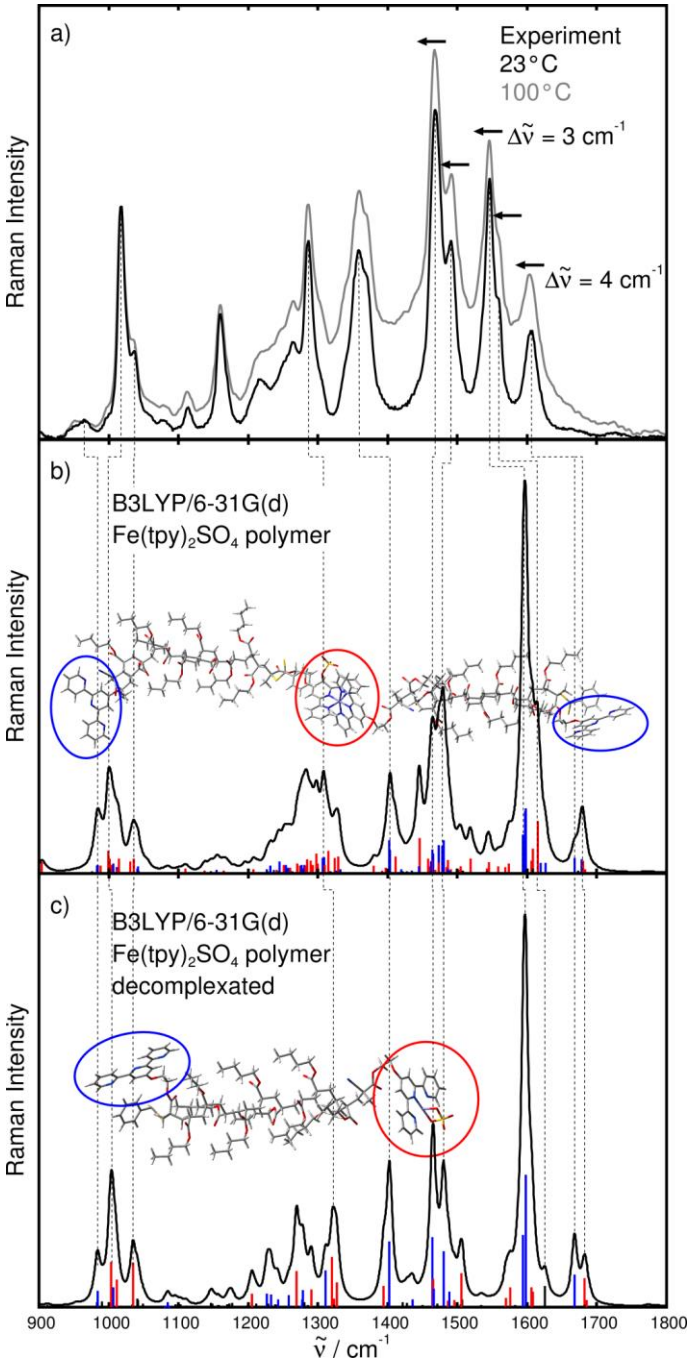

Raman spectra of the iron(II) sulfate metallopolymer. a) depicts temperature-dependent Raman spectra at 23 and 100 °C along with the thermally induced bathochromic shifts of the intensity pattern. b) and c) display calculated Raman spectra at the QM/MM level of theory using B3LYP and the 6-31G(d) basis set and the universal force field for two polymer models. Vibrational modes centered at the *bis*terpyridine-iron(II) complex are shown in red and modes of the free terminal terpyridine moieties are shown in blue.

Figure S8

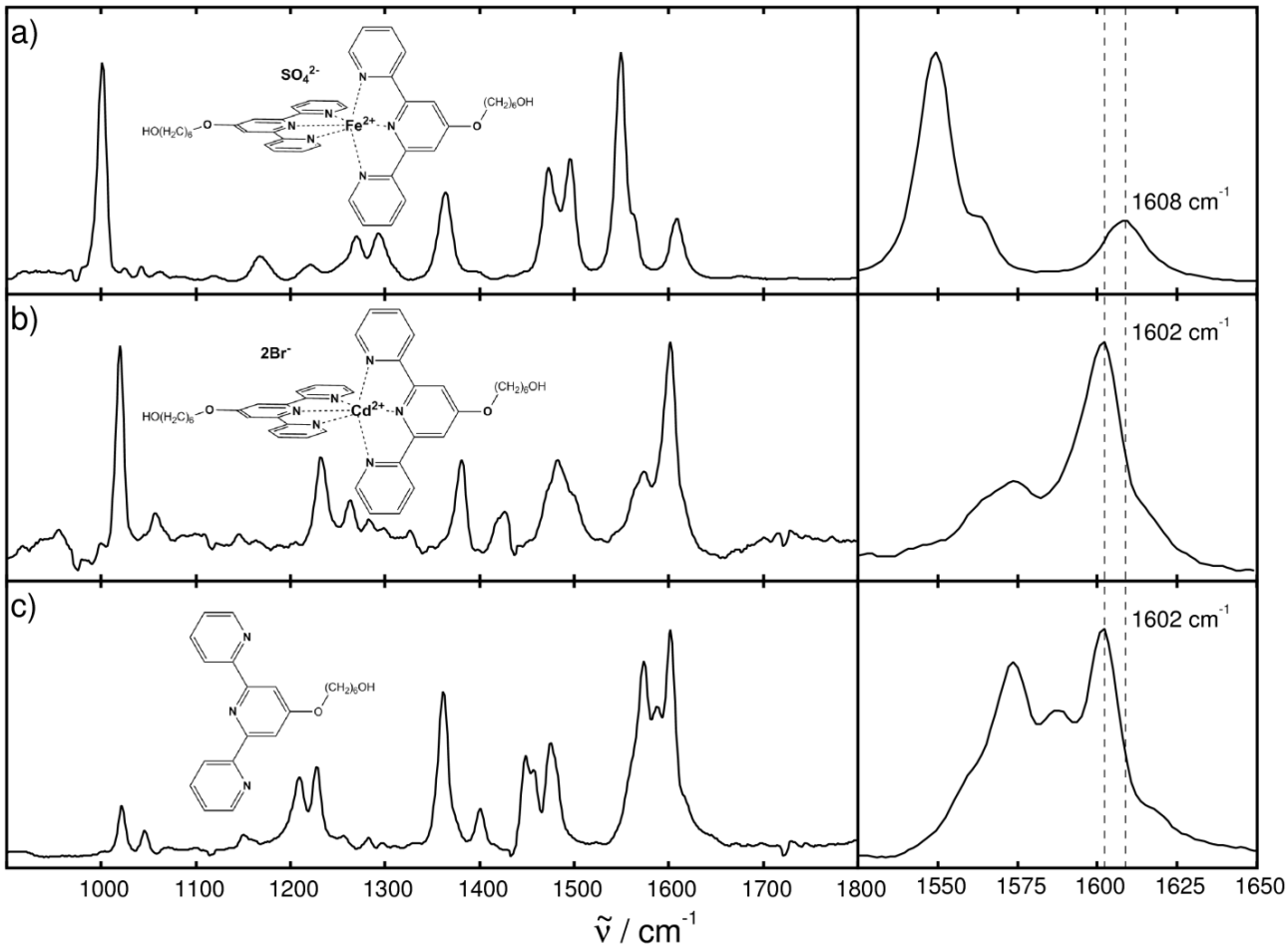

Raman spectra of the iron(II) sulfate a), cadmium(II) bromide b), and terpyridine c) monomers measured upon excitation at 568 nm. Raman frequencies for bands correlated to the observed bathochromic shifts of the metallopolymers are indicated.

Figure S9

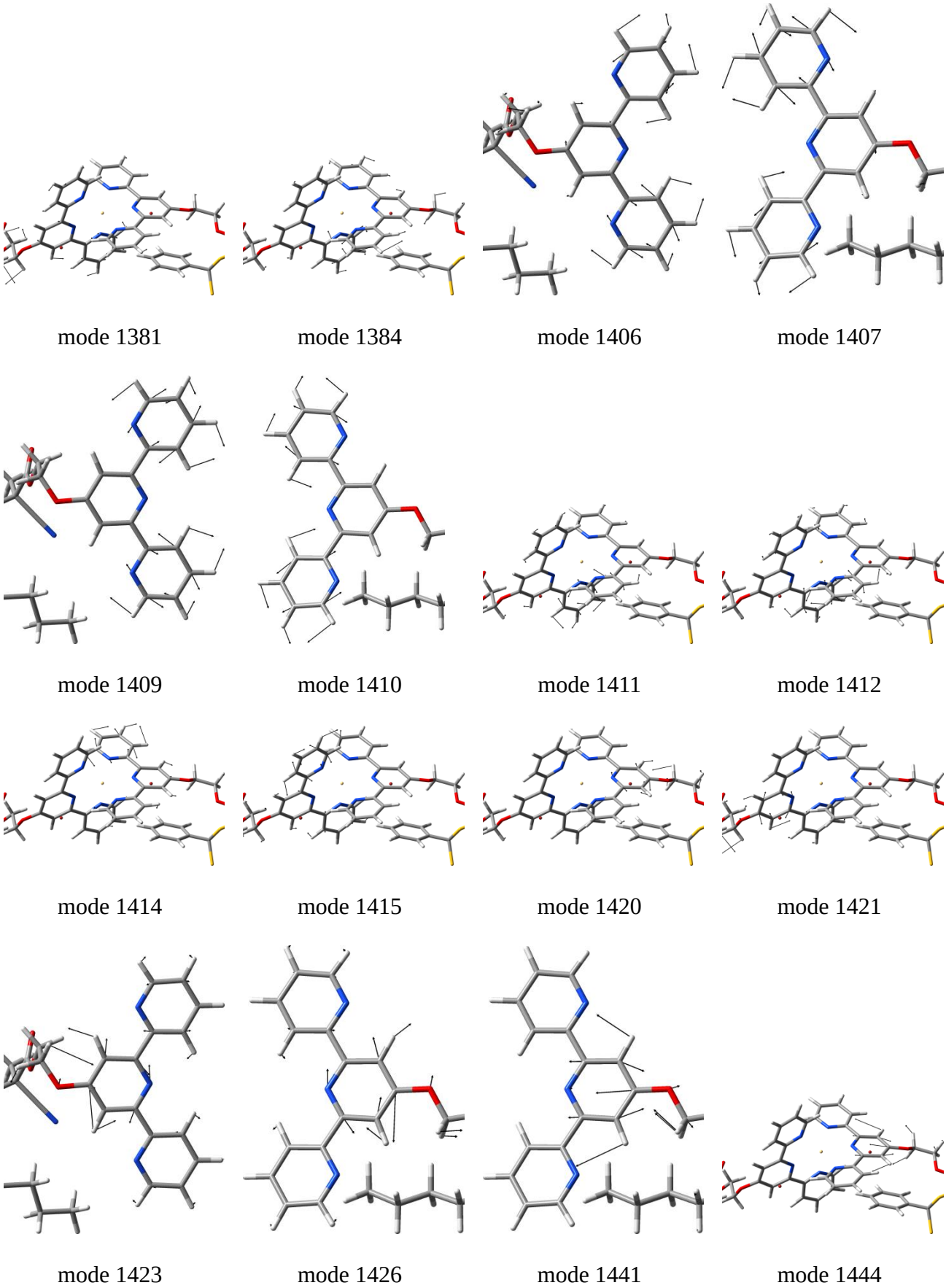

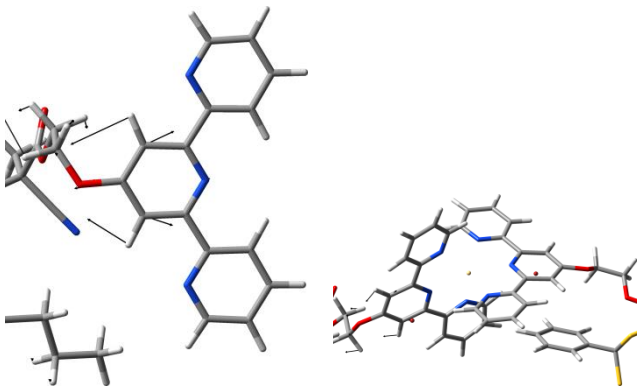

mode 1453 mode 1454

Intense vibrational modes of the cadmium(II) bromide metallopolymer contributing to the experimental Raman bands at 1597 and 1724 cm^{-1}.

Table S10

cadmium(II) bromide metallopolymer									
	B3LYP(15)/6-31G(d)			B3LYP(15)/6-311G(d)			B3LYP/6-31G(d)		
assignment	mode	$\tilde{\nu}$/ cm^{-1}	I / Å^{4}amu^{-1}	mode	$\tilde{\nu}$/ cm^{-1}	I / Å^{4}amu^{-1}	mode	$\tilde{\nu}$/ cm^{-1}	I / Å^{4}amu^{-1}
complex tpy sym	1381	1568.0	668	1370	1556.1	788	1402	1580.4	779
complex tpy sym	1384	1569.2	366	1373	1558.0	387	1403	1581.7	286
free tpy asym	1406	1581.3	333	1387	1569.2	308	1409	1593.8	341
free tpy asym	1407	1581.7	318	1389	1570.0	116	1411	1594.3	320
free tpy sym	1409	1584.9	593	1396	1572.6	341	1413	1597.5	555
free tpy sym	1410	1585.1	586	1398	1572.8	587	1414	1597.8	554
complex tpy asym	1411	1586.0	60	1408	1576.8	64	1415	1598.5	44
complex tpy asym	1412	1586.3	274	1409	1577.2	284	1416	1598.9	247
complex tpy sym	1414	1590.5	235	1412	1581.2	259	1418	1603.7	113
complex tpy sym	1415	1591.0	99	1413	1581.8	81	1419	1603.8	241
complex tpy asym	1420	1600.9	701	1415	1589.1	581	1421	1611.9	469
complex tpy asym	1421	1602.1	469	1418	1593.3	176	1424	1613.4	451
free tpy asym	1423	1608.7	96	1421	1597.5	73	1426	1419.2	93
free tpy asym	1426	1614.3	89	1423	1603.5	89	1427	1624.1	87
free tpy sym	1441	1658.1	143	1435	1649.9	149	1450	1667.9	140
complex tpy sym	1444	1663.6	62	1440	1656.4	63	1454	1674.9	74
free tpy sym	1453	1669.2	123	1444	1661.3	128	1455	1678.5	123
complex tpy sym	1454	1670.2	41	1449	1666.1	47	1465	1690.7	30

Assignment and comparison of the calculated vibrational frequencies (cm^{-1}) and relative Raman activities (Å^{4}amu^{-1}) for the iron(II) sulfate cross-linked metallopolymer as well as its semi-decomplexated form obtained at the B3LYP15/6-31G(d), B3LYP15/6-311G(d), and B3LYP/6-31G(d) levels of theory.

Figure S11

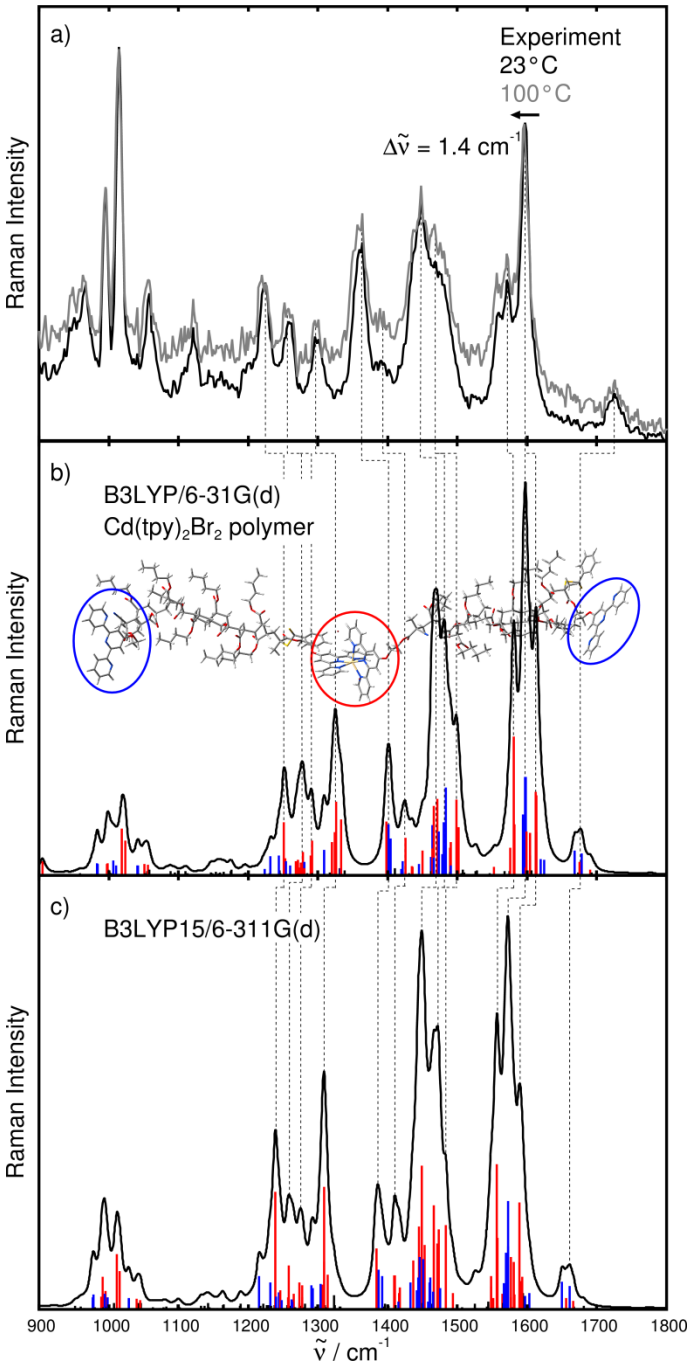

Raman spectra of the cadmium(II) bromide metallopolymer. a) depicts temperature-dependent Raman spectra at 23 and 100 °C along with the thermally induced bathochromic shifts of the intensity pattern. b) and c) display calculated Raman spectra at the QM/MM level of theory using B3LYP/6-31G(d) and B3LYP(15)/6-311G(d), respectively, and the universal force field the polymer models. Vibrational modes centered at the *bis*terpyridine-cadmium(II) complex are shown in red and modes of the free terminal terpyridine moieties are shown in blue.

Figure S12

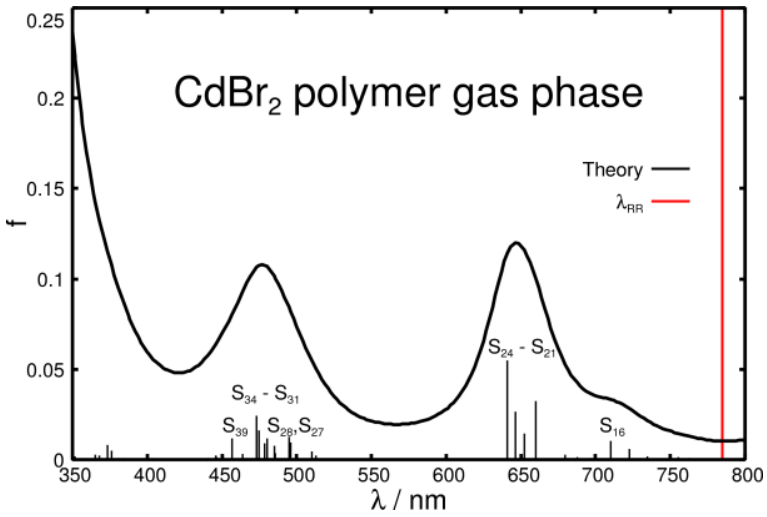

Simulated UV-vis spectrum of the cadmium(II) bromide metallopolymer in the gas phase performed at the QM/MM level of theory using TD-B3LYP(15) with the 6-31G(d) basis set and the UFF; the red line corresponds to excitation wavelength used in the Raman measurements.

Figure S13

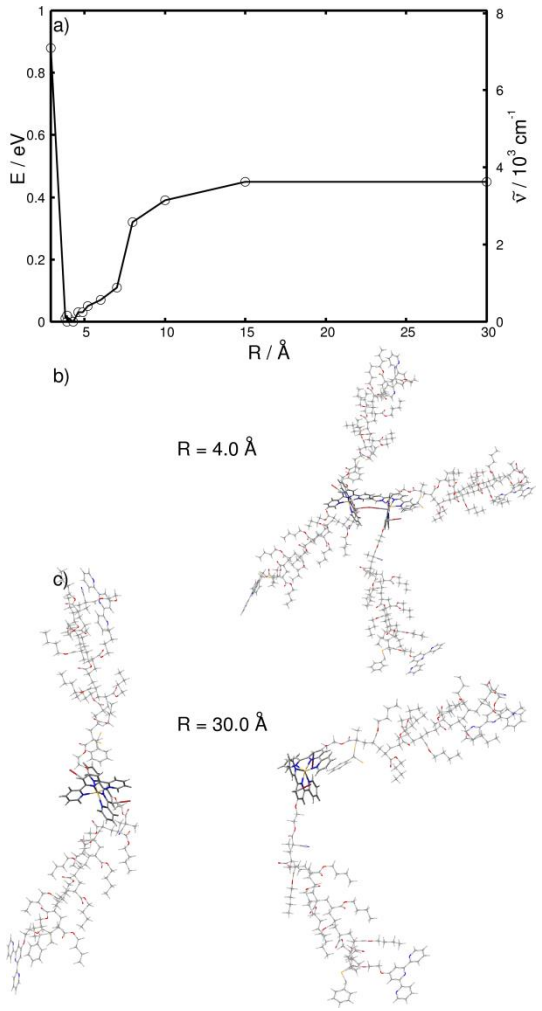

Calculation of the relaxed PES of the cadmium(II) bromide metallopolymer at the QM/MM level of theory using B3LYP(15) with the 6-31G(d) basis set and the universal force field with respect to the distance *R* describing the cleavage of the ionic cluster up to *R* = 30 Å. b) and c) depicts the global minimum of the PES (*R* = 4.0 Å) and the opened cluster at *R* = 30 Å in the orthogonal oriented conformation.